Eur. Phys. J. C (2021) 81:43
https://doi.org/10.1140/epjc/s10052-021-08844-z

THE EUROPEAN PHYSICAL JOURNAL C

Regular Article - Theoretical Physics

Triply charged Higgs bosons at a 100 TeV *pp* collider

Junxing Pan[1,a], **Jung-Hsin Chen**[2,b], **Xiao-Gang He**[1,2,3,4,c], **Gang Li**[2,5,d], **Jhih-Ying Su**[2,e]

[1] School of Physics and Information Engineering, Shanxi Normal University, Linfen 041004, China
[2] Department of Physics, National Taiwan University, Taipei 10617, Taiwan
[3] Tsung-Dao Lee Institute, and School of Physics and Astronomy, Shanghai Jiao Tong University, Shanghai 200240, China
[4] Physics Division, National Center for Theoretical Sciences, Hsinchu 30013, Taiwan
[5] Amherst Center for Fundamental Interactions, Department of Physics, University of Massachusetts Amherst, Amherst, MA 01003, USA

Received: 21 April 2020 / Accepted: 8 January 2021 / Published online: 18 January 2021

Abstract In this work, we study the potential of searching for triply charged Higgs boson originating from a complex Higgs quadruplet in the final state with at least three same-sign leptons. A detailed collider analysis of the SM backgrounds and signals is performed at a 100 TeV pp collider for the triply charged Higgs boson mass below 1 TeV and the Higgs quadruplet vacuum expectation value v_Δ ranging from 1.5×10^{-9} GeV to 1.3 GeV and the mass splitting Δm between the nearby states of the Higgs quadruplet satisfying $|\Delta m| \lesssim 30$ GeV. About 100 fb^{-1} of data are required at most for 5σ discovery. We also revisit the sensitivity at the Large Hadron Collider (LHC) and find that 5σ discovery of the triply charged Higgs boson below 1 TeV can be reached for a relatively small v_Δ. For example, if $v_\Delta = 10^{-6}$ GeV and $\Delta m = 0$, the integrated luminosity of 330 fb^{-1} is needed. But for a relatively large v_Δ, i.e., $v_\Delta \gtrsim 10^{-3}$ GeV, the triply charged Higgs boson above about 800 GeV cannot be discovered even in the high-luminosity LHC era. For $\Delta m > 0$, the cascade decays are open and the sensitivity can be improved depending on the value of v_Δ.

1 Introduction

The discovery of a neutral Higgs boson with mass around 125 GeV [1,2] was a great sucess of the Standard Model (SM) of particle physics. Nevertheless, the SM is not complete since it does not explain neutrino mass and cannot provide dark matter candidate, et al. Studies of new physics beyond the SM at colliders, such as precision tests of the Higgs boson and direct searches for additional Higgs bosons, can help us to answer these questions, since new physics may be closely connected to the Higg sector at TeV scale.

There are many highly motivated theoretical models, which predict more than one Higgs boson. The two-Higgs-doublet [3], minimal SUSY [4], and multi-Higgs doublet [5,6] models are some of the most studied models. In these models, there are not only new neutral Higgs bosons, but also singly charged Higgs boson. Electrically multi-charged Higgs bosons also exist in other well-motivated models, such as the doubly charged Higgs boson in the Type-II seesaw model [7–15], and even higher (multiple) charged Higgs boson in minimal dark matter models [16,17]. Since the mass splitting in the Higgs multiplet is small compared to the mass of a charged or neutral component itself, the discovery of any of these Higgs bosons can also provide indirect constraints on the other components. To this end, one needs to know how such color singlet multi-charged Higgs bosons can be produced and detected at colliders.

Before going to some detailed discussions, let us briefly discuss the main mechanism of producing multi-charged Higgs bosons and how they can be detected. We will indicate a color singlet higher dimensional Higgs boson H_n transforming under $SU(2)_L \times U(1)_Y$ as (n, Y). We will take values of Y such that the resulting electric charges of the Higgs bosons are zero or integers and write the component fields as h_n^Q with electric charge given by $Q = m + Y_n$. Here m is the third component of isospin I_n. The kinetic terms of the Higgs multiplet H_n and the SM Higgs doublet H are given by

$$\begin{aligned}\mathcal{L}_{\text{kinetic}} &= (D^\mu H)^\dagger D_\mu H + (D^\mu H_n)^\dagger D_\mu H_n \ , \\ D_\mu &= \partial_\mu + igT^a W_\mu^a + ig' Y B_\mu \\ &= \partial_\mu + i\frac{g}{\sqrt{2}}(T_+ W_\mu^+ + T_- W_\mu^-)\end{aligned}$$

[a] e-mail: panjunxing2007@163.com
[b] e-mail: lewis02030405@gmail.com
[c] e-mail: hexg@phys.ntu.edu.tw
[d] e-mail: ligang@umass.edu (corresponding author)
[e] e-mail: b02202013@ntu.edu.tw

$$+ie(T_3+Y)A_\mu + i\frac{g}{c_W}(T_3-(T_3+Y)s_W^2)Z_\mu\ , \tag{1}$$

where T^a is the $SU(2)_L$ generator for n-dimensional representation with the normalization $\mathrm{Tr}(T^aT^b)=\delta^{ab}/2$. $T_\pm$ are the raising and lowering operators, the operator $T_3h_n^Q = mh_n^Q$, $Yh_n^Q = Y_nh_n^Q$ and $e = gg'/\sqrt{g^2+g'^2}$ with g' and g being the $SU(2)_L$ and $U(1)_Y$ gauge couplings. The abbreviations $c_W \equiv \cos\theta_W$ and $s_W \equiv \sin\theta_W$ with θ_W being the weak mixing angle are used. The gauge interactions are the main interactions responsible for production of the multi-charged Higgs bosons.

The neutral components of H and H_n can be decomposed as $(v_H + h^0 + iI^0)/\sqrt{2}$ and $(v_n + h_n^0 + iI_n^0)/\sqrt{2}$. If H and H_n have non-zero vacuum expectation of values (VEVs) $v_H/\sqrt{2}$ and $v_n/\sqrt{2}$, the Z and $W^\pm$ will receive masses and the $SU(2)_L\times U(1)_Y$ will break down to $U(1)_{\rm em}$. Certain linear combinations of components in H and H_n will become the would-be Goldstone bosons G_Z and G_W^+ "eaten" by the Z and $W^\pm$ bosons. When discussing detecting physical Higgs bosons, these would-be Goldstone bosons should be separated and counted as longitudinal components of the Z and $W^\pm$ bosons. We provide details by expanding Eq. (1) in Appendix A.

After the would-be Goldstone bosons are removed, one can identify the physical degrees of freedom for the Higgs bosons and discuss their production. If there is only one Higgs multiplet H_n. The production of a multi-charged Higgs boson $h^{|Q|\pm}$[1] at a pp collider can happen in the following fashions: (1) the Drell-Yan type through the s-channel exchange of a virtual γ, Z or $W^\pm$ boson in $pp\to\gamma^*,\ Z^*\to h_n^{|Q|+}+h_n^{|Q|-}$ or $pp\to W^{\pm *}\to h_n^{|Q|\pm}h_n^{|Q-1|\mp}$; and (2) two vector boson fusion type through the pp collision to produce pair $\gamma\gamma$, γZ, ZZ, $(\gamma, Z)\ W^\pm$ or W^+W^- followed by $\gamma\gamma, \gamma Z, ZZ, W^+W^-\to h^{|Q|+}h^{|Q|-}$, or $(\gamma, Z)\ W^\pm\to h_n^{|Q|\pm}h_n^{|Q-1|\mp}$. Here the vector bosons are virtual, but the photons can be almost real at the LHC [18–20].

The multi-charged Higgs boson $h_n^{|Q|+}$ (similarly for $h_n^{|Q|-}$) produced can be detected by the decays $h_n^{|Q|+}\to h_n^{|Q-1|+}W^+\to\cdots\to h_n^{2+}\underbrace{W^+\cdots W^+}_{|Q-2|}$, where the multi-charged Higgs boson h_n^{q+} $(2\le q\le|Q-1|)$ and W^+ boson may be on shell or off shell. The decay of the doubly charged Higgs boson h_n^{2+} $(\equiv h_n^{++})$ is model dependent: it can decay into $h_n^+W^+$ or W^+W^+. In the former case, h_n^+ can be detected by $h_n^+\to\bar f f'$ with f and f' denoting lighter fermions, W^+h^0 followed by the decay of neutral Higgs boson h_n^0 into SM particles, or W^+Z if there exists at least one H_n representation with $n\ge 3$ [21,22]. If we consider the couplings of doubly charged Higgs boson to charged leptons, as in the Type-II seesaw model [7–11], the decay channel $h_n^{2+}\to\ell^+\ell^+$ can also be utilized. The decay $h_n^{|Q|+}\to h_n^{|Q-1|+}W^+\to\cdots\to h_n^0\underbrace{W^+\cdots W^+}_{|Q|}$ depends on the mass splitting between the charged Higgs bosons with $\Delta Q=\pm1$ and is independent of the VEV v_n. The widths of $h_n^+\to\bar f f'$, W^+Z and $h_n^{2+}\to W^+W^+$ however are proportional to v_n^2, and that of $h_n^{2+}\to\ell^+\ell^+$ is proportional to $1/v_n^2$.

If there exist the SM doublet H and Higgs multiplet H_n simultaneously, the singly charged Higgs boson h_n^+ and neutral Higgs boson h_n^0 above are not the mass eigenstates , see Eqs. (A5) (A7). However, since the VEV v_n is much smaller than v_H constrained by the ρ parameter [23],[2] h_n^+, h_n^0 are almost the same as the mass eigenstates if H_n is in the real representation.

There have been plenty phenomenological studies of singly, doubly and triply charged Higgs boson searches at the LHC. A review of thorough studies of singly charged Higgs boson in the two-Higgs-doublet models (2HDMs) can be found in Ref. [27]. Apart from the 2HDMs, singly charged Higgs bosons in models with weak singlet charged scalar and triplet models have also been investigated, which are characterized by sizable couplings to the first two generation fermions [28,29] and tree-level coupling to W^+Z [30], respectively. Doubly charged Higgs bosons have been studied, for example, in the Type-II seesaw model in $h_3^{2+}\to\ell^+\ell^+, h_3^+W^+, W^+W^+$ channels [12,13,18,31] and in the Georgi-Machacek model [32,33] in the $h_3^{2+}\to h_3^+W^+, W^+W^+$ channels [34,35]. For the triply charged Higgs boson, it has not been discussed as much as the charged Higgs bosons with smaller electric charges. To this end, we will take a specifically non-trivial model with a Higgs quadruplet ($n=4$, $Y_n=3/2$) to show how a triply charged Higgs boson can be detected in the following sections.

Triply charged Higgs boson in the model with a Higgs quadruplet was firstly investigated in Ref. [36], in which a mechanism for generating tiny neutrino masses at tree level via dimension-7 operators was proposed. The detailed phenomenology of triply charged Higgs boson in this model at the LHC were discussed in Refs. [37–39] with same-sign trilepton (SS3L) signature, that is at least three same-sign leptons in the final state. We will show in Sect. 5 that due to mis-interpretation of the significance formula in the literature, the discovery significance at the LHC was underestimated by several times in Refs. [37–39], so that the integrated luminosity required to reach 5σ discovery was overestimated by one or two orders. Besides, it is noted that although the final state with at least threee same-sign leptons was searched

[1] $h^{|Q|\pm}$ means a multi-charged Higgs boson with the electric charge being $\pm|Q|$ with $|Q|\ge1$.

[2] In some special cases with the VEVs satisfying $v_n=v_H$, $\rho=1$ is predicted at tree level for $n=2$ with $I=1/2$, $Y=1/2$ or $n=7$ with $I=3$, $Y=2$ [24–26].

at the LHC [40], additional b-jet, which is vetoed in our analysis, was also required [40].

When going beyond the LHC, there may be greater chance to discover multi-charged Higgs bosons. In this work we will first concentrate on the study of the discovery potential for the triply charged Higgs boson at a 100 TeV pp collider. After investigating the kinematic distributions at a 100 TeV pp collider and the LHC, we find that it is possible to project the results at a 100 TeV pp collider to the LHC without repeating the collider simulation. Our study shows that 5σ discovery can be reached for a triply charged Higgs boson below 1 TeV with 330 fb^{-1} of data at the LHC for a relatively small $v_\Delta = 10^{-6}$ GeV and with 110 fb^{-1} of data at a 100 TeV pp collider for the mass splitting $\Delta m = 0$. For $\Delta m > 0$, the sensitivity is further improved due to the cascade decays.

This paper is organized as follows: in Sect. 2, details of the model with a Higgs quadruplet and vector-like triplet leptons are given. In Sect. 3, current (indirect) constraints on this model are discussed. In Sect. 4, we discuss the production and decay of the triply charged Higgs boson, where the cascade decays are systematically studied. In Sect. 5, a detailed collider analysis is performed at a 100 TeV pp collider and the sensitivity at the LHC is revisited. Sect. 6 summarizes our results.

2 A triply charge Higgs boson model

We now provide some information about the triply charged Higgs boson in a complex Higgs quadruplet $\Delta \sim (1, 4, 3/2)$ into the SM to be studied, which is expressed as $\Delta = (\Delta^{+++}, \Delta^{++}, \Delta^{+}, \Delta^{0})^T$, the scalar kinetic Lagrangian is shown in Eq. (1) with $\Delta = H_n$. The covariant derivatives

$$D_\mu \Delta = (\partial_\mu - igT^a W_\mu^a - ig' Y_\Delta B_\mu)\Delta, \tag{2}$$

$$D_\mu H = (\partial_\mu - ig\tau^a W_\mu^a - ig' Y_H B_\mu)H, \tag{3}$$

and the Higgs doublet $H \sim (1, 2, 1/2)$ is given by $H = (H^+, H^0)^T$. The hypercharges $Y_\Delta = 3/2$, $Y_H = 1/2$, and the matrices τ^a and T^a denote the $SU(2)$ generators in the doublet and quadruplet representations, respectively.

The Higgs potential is expressed as [36]

$$\begin{aligned} V(H, \Delta) = & -\mu_H^2 H^\dagger H + \mu_\Delta^2 \Delta^\dagger \Delta \\ & + \lambda_1 (H^\dagger H)^2 + \lambda_2 (\Delta^\dagger \Delta)^2 \\ & + \lambda_3 (H^\dagger H)(\Delta^\dagger \Delta) + \lambda_4 (H^\dagger \tau^a H)(\Delta T^a \Delta) \\ & + (\lambda_5 H^3 \Delta^* + \text{H.C.}) \,. \end{aligned} \tag{4}$$

The last term is explicitly written as $\lambda_5 H_a H_b H_c \Delta^*_{abc} + \text{H.C.}$ with the totally symmetric tensors

$$H_1 = H^+, \quad H_2 = H^0, \tag{5}$$

$$\Delta_{111} = \Delta^{+++}, \quad \Delta_{112} = \frac{1}{\sqrt{3}}\Delta^{++},$$
$$\Delta_{122} = \frac{1}{\sqrt{3}}\Delta^{+}, \quad \Delta_{222} = \Delta^0 \,. \tag{6}$$

After the electroweak symmetry breaking, $H^0 \to (v_H + h^0)/\sqrt{2}$ and $\Delta^0 \to (v_\Delta + h^0_\Delta)/\sqrt{2}$. One obtains that VEVs of the fields H and Δ,

$$v_H = \sqrt{\frac{\mu_H^2}{\lambda_1}}, \quad v_\Delta = -\frac{v_H^3 \lambda_5}{2m_\Delta^2} \,. \tag{7}$$

Here m_Δ denotes the mass of the neutral field h^0_Δ of the quadruplet Δ,

$$m_\Delta^2 = \mu_\Delta^2 + \frac{1}{8} v_H^2 (4\lambda_3 + 3\lambda_4) \,. \tag{8}$$

We can see from the Higgs potential that the λ_4 term induces the mass splitting between the nearby states of the Higgs quadruplet. To be more concrete, the mass of the field[3] Δ^{n+}, is given by

$$m^2_{\Delta^{n+}} = m_\Delta^2 - n\frac{\lambda_4}{4} v_H^2 \,. \tag{9}$$

The singly charged states $H^\pm$ and $\Delta^\pm$ can mix with each other, thus it is necessary to define the normalized and orthogonal states via

$$\begin{pmatrix} G_W^\pm \\ \phi^\pm \end{pmatrix} = 1/v \begin{pmatrix} v_H & \sqrt{3}v_\Delta \\ -\sqrt{3}v_\Delta & v_H \end{pmatrix} \begin{pmatrix} H^\pm \\ \Delta^\pm \end{pmatrix} \tag{10}$$

with $v \equiv \sqrt{v_H^2 + 3v_\Delta^2} \simeq 246$ GeV, where $G_W^\pm$ and $\phi^\pm$ are the would-be Goldstone boson and physical singly charged Higgs boson, respectively. The electroweak ρ parameter is equal to $(v_H^2 + 3v_\Delta^2)/(v_H^2 + 9v_\Delta^2)$ in this model. After removing the Goldstone mode, one obtains interactions of the physical singly charged Higgs boson $\phi^\pm$ to SM fermions and gauge bosons. With the experimental measurement of ρ [23], one obtains $v_\Delta \lesssim 1.3$ GeV at 3σ level. Since the mixing effects are highly suppressed by v_Δ/v, we will not consider them but keep in mind that singly charged Higgs boson can couple to SM leptons even if there are no other fields being introduced. Similarly, neutral Higgs bosons from the doublet and quadruplet can also mix, depending on the parameter λ_5 in the Higgs potential. For $v_\Delta \ll v$, the mass eigenstates of neutral Higgs bosons are

$$\begin{pmatrix} h_1^0 \\ h_2^0 \end{pmatrix} = 1/\sqrt{v_H^2 + 9v_\Delta^2} \begin{pmatrix} v_H & 3v_\Delta \\ 3v_\Delta & -v_H \end{pmatrix} \begin{pmatrix} h^0 \\ h^0_\Delta \end{pmatrix} \,, \tag{11}$$

[3] Here, $\Delta^{1+} = \Delta^+$, $\Delta^{2+} = \Delta^{++}$, and $\Delta^{3+} = \Delta^{+++}$.

where h_1^0 is identified as the discovered Higgs boson with mass of about 125 GeV.

Motivated by the non-zero neutrino masses, we consider the scenario, in which a pair of vector-like triplet leptons $\Sigma_{L,R} \sim (1,3,1)$ with $\Sigma = (\Sigma^{++}, \Sigma^{+}, \Sigma^{0})^T$ are introduced into the SM [36]. This enables the quadruplet Higgs boson to couple to SM leptons after integrating out the heavy $\Sigma_{L,R}$. The Yukawa Lagrangian is described as

$$\mathcal{L}_{\rm Yuk} = Y_i \overline{L_{ia}^c} \epsilon^{aa'} \Sigma_{La'b} H_b^* + \overline{Y}_i \overline{\Sigma_{Rab}} \Delta_{abc} L_{ic'} \epsilon^{cc'} \,, \quad (12)$$

where L is the left-handed lepton doublet, Y_i and $\bar{Y}_i$ are the Yukawa couplings with i being the generation index. The total symmetric tensors

$$\Sigma_{11} = \Sigma^{++}, \quad \Sigma_{12} = \frac{1}{\sqrt{2}}\Sigma^{+}, \quad \Sigma_{22} = \Sigma^{0} \,. \quad (13)$$

Integrating out $\Sigma_{L,R}$, we obtain the dimension-5 effective operator

$$\mathcal{L}_{\rm Yuk}^{\rm eff} = -\frac{Y_i \overline{Y}_j + Y_j \overline{Y}_i}{m_\Sigma} \overline{L_{ia}^c} L_{ja'} H_b^* \Delta_{bcd} \epsilon^{ac'} \epsilon^{a'd} + \text{H.C.} \,, \quad (14)$$

where m_Σ is the mass of Σ fields. Assuming that the neutrino mass is generated by the above interaction, we obtain

$$\mathcal{L}_{\rm Yuk}^{\rm eff} \supset \frac{(m_\nu)_{ij}}{v_\Delta} \left(\overline{\nu_{Li}^c} \nu_{Lj} \frac{v_\Delta}{2} - \overline{\nu_{Li}^c} \ell_{Lj} \frac{\Delta^+}{\sqrt{6}} - \overline{\ell_{Li}^c} \nu_{Lj} \frac{\Delta^+}{\sqrt{6}} + \overline{\ell_{Li}^c} \ell_{Lj} \frac{\Delta^{++}}{\sqrt{6}} \right) + \text{H.C.}. \quad (15)$$

The first term gives rise to neutrino masses in the flavor basis, the second and third terms contribute to the singly charged Higgs boson decaying into leptons, and the fourth term induces the leptonic decay of the doubly charged Higgs boson as we will discuss in detail in Sect. 4.2.

3 Constraints

In this section, we will discuss indirect constraints on the model with an extended Higgs quadruplet proposed in Sect. 2 from the decay of Higgs boson into $\gamma\gamma$, the electroweak precision tests (EWPTs), perturbativity, and low-energy rare processes $\mu \to e\gamma$ decay and μ-e conversion. It is well known that charged Higgs bosons can contribute at 1-loop level to the decay of $h_1^0 \to \gamma\gamma$, which has been measured by the ATLAS and CMS Collaboration and combined in terms of signal strengths $\mu_{\gamma\gamma}^{\rm ATLAS} = 1.06 \pm 0.12$ [41] and $\mu_{\gamma\gamma}^{\rm CMS} = 1.20^{+0.17}_{-0.14}$ [42] with the integrated luminosities of 80 fb^{-1} and 35.9 fb^{-1}, respectively. Due to the larger integrated luminosity, we will take the combined signal strength $\mu_{\gamma\gamma}^{\rm ATLAS}$ to constrain the model parameters.

The couplings between h_1^0 and charged Higgs bosons $\Delta^{n\pm}$, i.e,, $h_1^0 \Delta^{n+} \Delta^{n-}$, are

$$\tilde{\lambda}_n = v_H \left(\lambda_3 + \frac{3-2n}{4} \lambda_4 \right), \quad n = 1, 2, 3 \,. \quad (16)$$

From Eq. (9), one sees that λ_4 is fixed by the mass splitting Δ, which is given by

$$\lambda_4 = \frac{8 m_\Delta}{v_H^2} \Delta m. \quad (17)$$

The partial width of $h_1^0 \to \gamma\gamma$ is thus modified as [43],

$$\frac{\Gamma(h_1^0 \to \gamma\gamma)}{\Gamma(h_1^0 \to \gamma\gamma)_{\rm SM}} = \frac{\left| N_c Q_t^2 A_{1/2}(\tau_t) + A_1(\tau_W) + \sum_{n=1}^{3} \frac{v_H \tilde{\lambda}_n Q_n^2}{2 m_{\Delta^{n\pm}}^2} A_0(\tau_{\Delta^{n\pm}}) \right|^2}{|N_c Q_t^2 A_{1/2}(\tau_t) + A_1(\tau_W)|^2} \,, \quad (18)$$

where $\tau_t = m_{h_1^0}^2/(4m_t^2)$, $\tau_W = m_{h_1^0}^2/(4m_W^2)$ and $\tau_{\Delta^{n\pm}} = m_{h_1^0}^2/(4m_{\Delta^{n\pm}}^2)$,

$$A_{1/2}(\tau_i) = 2\big[\tau_i + (\tau_i - 1) f(\tau_i)\big]\tau_i^{-2} \,, \quad (19)$$

$$A_1(\tau_i) = -[2\tau_i^2 + 3\tau_i + 3(2\tau_i - 1) f(\tau_i)]\tau_i^{-2} \,, \quad (20)$$

$$A_0(\tau_i) = -\big[\tau_i - f(\tau_i)\big]\tau_i^{-2} \,, \quad (21)$$

and the function $f(\tau_i) = \arcsin^2 \sqrt{\tau_i}$ for $\tau_i < 1$. In Eq. (18), we have neglected the terms proportional to v_Δ/v_H.

Following Ref. [39], we also consider the indirect constraints from the EWPTs [44] by considering modification to the oblique parameters [45,46] and perturbativity, $\lambda_4 \le \sqrt{4\pi}$. In Fig. 1, we show the indirect constraints, which are almost independent of v_Δ, in the plane of $m_{\Delta^{\pm\pm\pm}}$ and Δm. For the $h_1^0 \to \gamma\gamma$ measurements, we consider the combined signal strength by the ATLAS Collaboration. The pink regions are excluded at 2σ confidence level (C.L.), where two benchmark values of the coupling $\lambda_3 = 1, 0.1$ are depicted. The cyan regions are excluded at 2σ C.L. by the perturbativity requirement. The regions between blue curves are however allowed at 2σ C.L. by the EWPTs. Thus there is still large room in the range of $|\Delta m| \lesssim 30$ GeV satisfying indirect constraints.

Charged Higgs bosons can contribute to other processes or observables at one-loop level [47]. The 90% C.L. upper

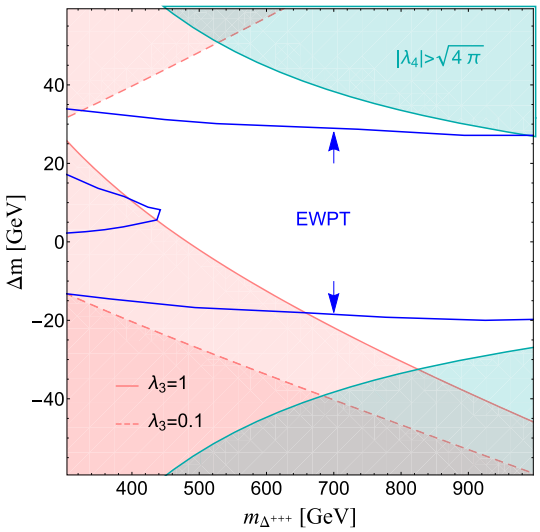

Fig. 1 Indirect constraints from $\mu_{\gamma\gamma}^{\rm ATLAS} = 1.06 \pm 0.12$, EWPT (taken from Ref. [39]) and perturbativity in the plane of $m_{\Delta^{\pm\pm\pm}}$ and Δm. Pink and cyan regions excluded at 2σ C.L., while the region between blue curves are allowed at 2σ C.L.. The pink regions with boundaries depicted in solid and dashed curves correspond to $\lambda_3 = 1$ and 0.1, respectively

limits on the decay branching ratio of $\mu \to e\gamma$ and rate of μ-e conversion are [48,49]

$$\begin{aligned} &{\rm Br}(\mu^+ \to e^+\gamma) \le 4.2 \times 10^{-13}, \\ &R(\mu N \to eN) \le 7 \times 10^{-13} \quad \text{for Au.} \end{aligned} \tag{22}$$

The decay branching ratio of $\mu \to e\gamma$ [50] and the conversion rate of μ-e [51,52] induced by charged Higgs bosons are given by

$${\rm Br}(\mu^+ \to e^+\gamma) = \frac{\alpha [(m_\nu^\dagger m_\nu)_{12}]^2}{108\pi G_F^2 v_\Delta^4} \left(\frac{1}{m_{\Delta^{\pm\pm}}^2} + \frac{1}{4m_{\Delta^\pm}^2} \right)^2 , \tag{23}$$

$$R(\mu N \to eN) = (4\pi\alpha)^2 \frac{2G_F^2 m_\mu^5}{\Gamma_{cap}} \times \left(A_R \frac{D}{\sqrt{4\pi\alpha}} + A_L V_p \right)^2 , \tag{24}$$

where α and G_F are the fine-structure constant and Fermion coupling constant, m_ν is the neutrino mass matrix in the flavor basis, and $D = 0.189$, $V_p = 0.0974$, $\Gamma_{cap} = 13.07 \times 6.58211814 \times 10^{-19}$ GeV [53]. Here,

$$A_R = -\frac{1}{\sqrt{2}G_F} \frac{(m_\nu^\dagger m_\nu)_{12}}{288\pi^2 v_\Delta^2} \left(\frac{1}{4m_{\Delta^\pm}^2} + \frac{1}{m_{\Delta^{\pm\pm}}^2} \right) , \tag{25}$$

$$A_L = -\frac{1}{\sqrt{2}G_F} \sum_{i=1,2,3} \frac{(m_\nu)_{i1}^* (m_\nu)_{i2}}{36\pi^2 v_\Delta^2} \left[\frac{1}{6m_{\Delta^\pm}^2} + \frac{1}{8m_{\Delta^{\pm\pm}}^2} f\left(\frac{m_\mu^2}{m_{\Delta^{\pm\pm}}^2}, \frac{m_i^2}{m_{\Delta^{\pm\pm}}^2} \right) \right] , \tag{26}$$

with $m_1 = m_e$, $m_2 = m_\mu$, $m_3 = m_\tau$, and the function

$$f(r,s) = \frac{4s}{r} + \ln(s) + \left(1 - \frac{2s}{r}\right) \sqrt{1 + \frac{4s}{r}} \ln \frac{\sqrt{r+4s} + \sqrt{r}}{\sqrt{r+4s} - \sqrt{r}} \tag{27}$$

In Fig. 2, the constraints from $\mu \to e\gamma$ and μ-e conversion measurements are shown. We obtain the most stringent constraint $v_\Delta \gtrsim 1.5 \times 10^{-9}$ GeV from $\mu^+ \to e^+\gamma$.

The triply charged Higgs boson mass and the mass splitting can also be bounded from direct searches for doubly charged Higgs bosons at the LHC. Doubly charged Higgs bosons in these searches are assumed to decay into a pair of same-sign leptons [54,55] or W bosons [56]. It has been shown in Refs. [38,39] that doubly charged Higgs searches can exclude the region of $m_{\Delta^{\pm\pm\pm}} \lesssim 400 - 600$ GeV depending on the VEV v_Δ. While it is important to include these constraints for a complete model study, we will concentrate

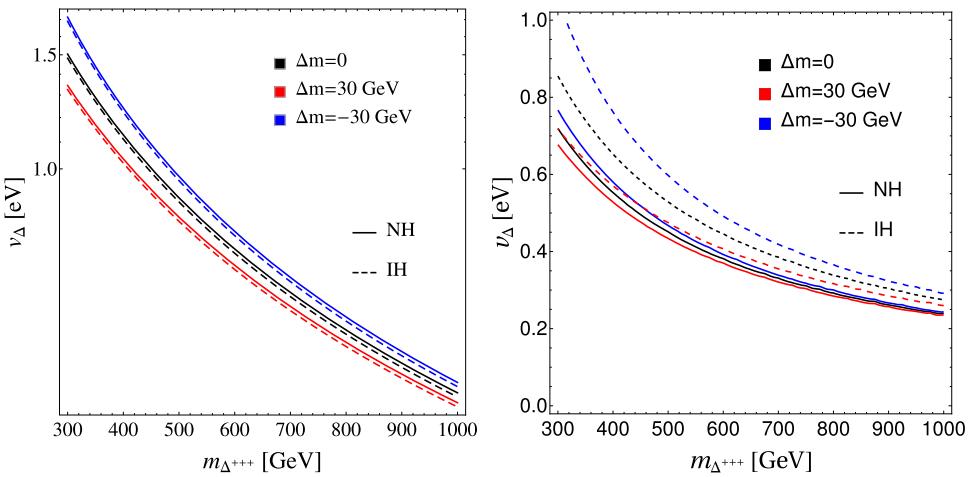

Fig. 2 Indirect constraints from $\mu \to e\gamma$ and μ-e conversion measurements in the plane of $m_{\Delta^{\pm\pm\pm}}$ and v_Δ. Regions below the curves are excluded at 90% C.L.. Solid and dashed curves correspond to the NH and IH, respectively. Black, red and blue curves are obtained with $\Delta m = 0$, 30 GeV and -30 GeV, respectively

on the sensitivities to triply charged Higgs boson searches at colliders with the model in Sect. 2 as a benchmark model with the mass region up to 1 TeV.

4 Production and decay of triply charged Higgs boson

4.1 Production cross sections

As mentioned in Sect. 1, triply charged Higgs bosons can be pair produced or associated produced with a doubly charged Higgs boson. In the s-channel, they correspond to the Drell-Yan processes through an off-shell photon or Z boson and through a W boson, which are termed "DYZ" and "DYW" processes hereafter, respectively. In the t-channel, charged Higgs bosons are produced in conjunction with two additional forward jets at leading order [18] by exchange of γ, Z and/or W boson. It was found in Refs. [18,20] that the photon fusion (PF) process with collinear initial photons dominates over other contributions involving off-shell photon, Z boson and/or W boson, named as vector boson fusion (VBF) process at the LHC. Following Refs. [18–20], we use an effective photon approximation [57] to describe the PF process, which includes elastic, semi-elastic, and inelastic sub-processes but loses potential tagging forward jets. Since the cross section of PF process is proportional to Q_Δ^4 with Q_Δ being the electric charge of $\Delta^{n\pm}$, it can even surpass the cross sections of DY processes for the production of triply charged Higgs boson. On the other hand, the VBF process, the cross section of which is expected to increase fairly with the collider energy, can be separated by tagging the forward jets and thus will not be considered in this work.

The studies of triply charged Higgs boson at the LHC with the center-of-mass energy $\sqrt{s} = 13 \sim 14$ TeV can be found in Refs. [37–39]. In the potential era of LHC update, named as High Energy LHC (HE-LHC) [58,59], the collider energy can reach 27 TeV, which increases the LHC mass reach of triply charged Higgs boson. A 100 TeV pp collider such as proton-proton Future Circular Collider (FCC-hh) [60,61] or Super Proton-Proton Collider (SPPC) [62,63] is also designed, which provides new possibilities of discovering triply charged Higgs bosons at pp colliders.

In the left panel of Fig. 3 we show the cross sections of triply charged Higgs production at $\sqrt{s} = 13$, 27 and 100 TeV obtained with `MG5_aMC@NLO v2.6.5` [64] and `NNPDF23_lo_as_0130_qed` PDF set [65] for the charged Higgs boson mass range between 300 GeV and 1000 GeV[4]. It is notable that the DY cross sections have been multiplied by a next-to leading order (NLO) K-factor of 1.25 [66,67], while higher order corrections to the PF process are small and neglected [18]. We can see that the cross section increases with the center-of-mass energy $\sqrt{s}$; the PF cross section dominates over the DY cross sections for $m_{\Delta^{\pm\pm\pm}} \lesssim$ 400 and 500 GeV at $\sqrt{s} = 13$ and 27 TeV, respectively, while at $\sqrt{s} = 100$ TeV the PF cross section is always smaller than the DY cross sections for $m_{\Delta^{\pm\pm\pm}} \leq 1000$ GeV [5]. The ratios of cross sections at $\sqrt{s} = 27$ TeV and $\sqrt{s} = 100$ TeV to that at $\sqrt{s} = 13$ TeV, denoted as σ_{100}/σ_{13} and σ_{27}/σ_{13}, are depicted in the right panel, which highlights the improvement of mass reach at $\sqrt{s} = 27$ and 100 TeV. We will postpone a detailed analysis at the HE-LHC to a future work.

4.2 Decays of charged Higgs bosons

To evaluate the significance of the production processes, it is essential to investigate the decays of charged Higgs bosons. Triply charged Higgs boson can decay in cascade into doubly charged Higgs boson or in three-body through an off-shell doubly charged Higgs boson. Therefore, we will first discuss the decay of doubly charged Higgs boson.

One can easily obtain the decay widths of doubly charged Higgs boson into W^+W^+ and $\ell^+\ell^+$ by rescaling those in the Type-II seesaw model [12–15], which are

$$\begin{aligned}\Gamma(\Delta^{\pm\pm} \to \ell_i^\pm \ell_j^\pm) &= \frac{m_{\Delta^{\pm\pm}}}{12\pi(1+\delta_{ij})}|h_{ij}|^2,\\ \Gamma(\Delta^{\pm\pm} \to W^\pm W^\pm) &= \frac{3g^4 v_\Delta^2 m_{\Delta^{\pm\pm}}^3}{64\pi m_W^4}\sqrt{1-4\xi_W}\\ &\quad (1-4\xi_W+12\xi_W^2)\end{aligned} \tag{28}$$

with $\xi_W \equiv m_W^2/m_{\Delta^{\pm\pm}}^2$, $\ell_{1,2,3} = e, \mu, \tau$, where we have defined [13]

$$h_{ij} = m_\nu^{ij}/(\sqrt{2}v_\Delta) \tag{29}$$

with m_ν^{ij} denoting the neutrino mass matrix in the flavor basis and assumed $m_{\Delta^{\pm\pm}} > 2m_W$. Here, we only consider the contribution of a Higgs quadruplet to neutrino mass at tree level; for 1-loop level contribution, one could refer to Refs. [37–39]. In the neutrino mass basis, the diagonal neutrino mass matrix is

$$m_\nu^{\rm diag} = U^T m_\nu U\ , \tag{30}$$

[4] In Fig. 3, we have set the masses of all the charged Higgs bosons to be the same, namely the mass splitting $\Delta m = 0$. For $\Delta m \neq 0$, the production cross section of the DYW process is altered. We have checked that for 300 GeV $\leq m_{\Delta^{\pm\pm\pm}} \leq$ 1000 GeV, the DYW production cross section is reduced by at most 5% for $\Delta m = 10$ GeV and 15% for $\Delta m = 30$ GeV.

[5] It is worthy to note that there is a large uncertainty of photon PDF in `NNPDF23_lo_as_0130_qed` PDF set, which could overestimate the photon-fusion production cross section at the LHC [68,69], but the impact is small at a 100 TeV pp collider since the dominant contribution comes from the DY processes.

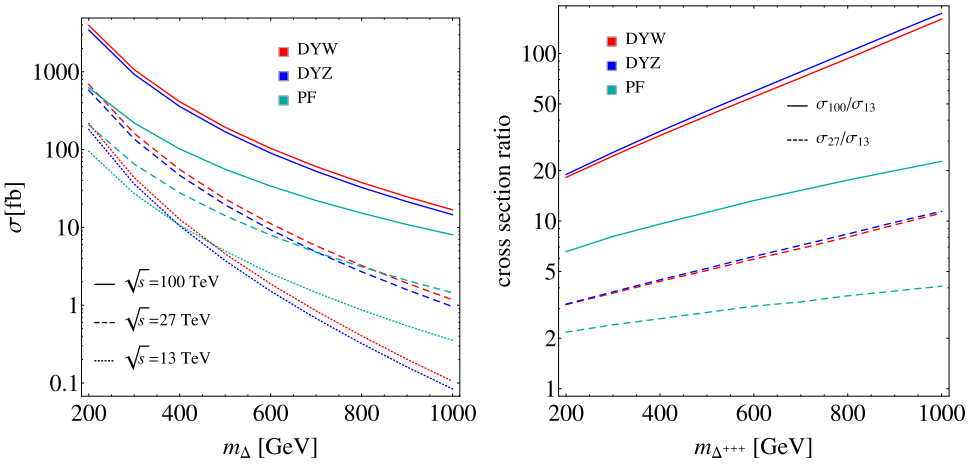

Fig. 3 Left: Production cross sections of triply charged Higgs bosons via the Drell-Yan processes (DYW, DYZ) and photon fusion process (PF) at $\sqrt{s} = 13$, 27 and 100 TeV as a function of $m_{\Delta^{\pm\pm\pm}}$ with the mass splitting neglected. Right: ratios of cross sections at $\sqrt{s} = 27$ and 100 TeV to that at $\sqrt{s} = 13$ TeV, denoted as σ_{27}/σ_{13} and σ_{100}/σ_{13}, respectively

where U is the Pontecorvo-Maki-Nakagawa-Sakata (PMNS) mixing matrix. Assuming that the CPV phases in the PMNS matrix are zero, we can determine the explicit form of m_ν using the central values of recent data [23][6] on the mixing angles and neutrino mass squared differences for both normal hierarchy (NH) and inverted hierarchy (IH) mass spectra.

Doubly charged Higgs boson $\Delta^{\pm\pm}$ can also decay into singly or triply charged Higgs boson, depending on the mass spectrum of the Higgs quadruplet. There are two cases for the mass spectrum, which is determined by the parameter λ_4 in the Higgs potential, see Eq. (9). Defining the mass splitting between the nearby states of the Higgs quadruplet, $\Delta m \equiv m_{\Delta^{\pm\pm}} - m_{\Delta^{\pm\pm\pm}} = m_{\Delta^\pm} - m_{\Delta^{\pm\pm}} = m_\Delta - m_{\Delta^\pm}$, we obtain

- Case $\Delta m > 0$: $m_{\Delta^{\pm\pm\pm}} < m_{\Delta^{\pm\pm}} < m_{\Delta^\pm} < m_\Delta$;
- Case $\Delta m < 0$: $m_{\Delta^{\pm\pm\pm}} > m_{\Delta^{\pm\pm}} > m_{\Delta^\pm} > m_\Delta$.

For case $\Delta m > 0$, $\Delta^{\pm\pm}$ can decay into $\Delta^{\pm *}W^\pm$, $\Delta^{\pm\pm\pm *}W^\mp$ and $\Delta^{\pm\pm\pm}W^{\mp *}$, while for case $\Delta m < 0$, $\Delta^{\pm\pm}$ can decay into $\Delta^{\pm\pm\pm *}W^\mp$, $\Delta^{\pm *}W^\pm$ and $\Delta^\pm W^{\pm *}$. Here, $\Delta^{\pm\pm\pm *}$, $\Delta^{\pm *}$ and $W^{\pm *}$ denote off-shell particles. The decay $\Delta^{\pm\pm} \to \Delta^{\pm *}W^\pm$ depends on the couplings of $\Delta^\pm W^\mp Z$ and $\Delta^\pm \ell^\mp \nu$, which are proportional to v_Δ or $1/v_\Delta$ similar to $\Delta^{\pm\pm} \to W^\pm W^\pm$ or $\Delta^{\pm\pm} \to \ell^\pm \ell^\pm$. Therefore, we can neglect the contribution of $\Delta^{\pm\pm} \to \Delta^{\pm *}W^\pm$ in the total width of $\Delta^{\pm\pm}$. The decay $\Delta^{\pm\pm} \to \Delta^{\pm\pm\pm *}W^\mp$ depends on the interaction of $\Delta^{\pm\pm\pm}$ to SM particles through an off-shell $\Delta^{\pm\pm}$ and can also be neglected.

The cascade decays $\Delta^{\pm\pm} \to \Delta^\pm W^{\pm *}$ and $\Delta^{\pm\pm} \to \Delta^{\pm\pm\pm}W^{\mp *}$ only depend on the mass splitting Δm approximately with the widths being given by [12,13]

$$\Gamma(\Delta^{\pm\pm} \to \Delta^\pm W^{\pm *}) = -\frac{3g^4 \Delta m^5}{40\pi^3 m_W^4}\,, \tag{31}$$

[6] There is an update of the mixing $\sin^2\theta_{23}$ [70], which slightly changes the neutrino mass matrix m_ν.

$$\Gamma(\Delta^{\pm\pm} \to \Delta^{\pm\pm\pm}W^{\mp *}) = \frac{9g^4 \Delta m^5}{160\pi^3 m_W^4}\,. \tag{32}$$

From the constraints by the EWPTs, $|\Delta m| \lesssim 30$ GeV as shown in Fig. 1. We will thus choose the benchmark values $\Delta m = 0, \pm 1$ GeV, ± 10 GeV for simplicity.

For $\Delta m < 0$ ($\Delta m > 0$), $\Delta^{\pm\pm}$ can also decay into $\Delta^\pm \pi^\pm$ ($\Delta^{\pm\pm\pm}\pi^\mp$) with the decay widths [12]

$$\Gamma(\Delta^{\pm\pm} \to \Delta^\pm \pi^\pm) = -\frac{g^4 \Delta m^3 f_\pi^2}{8\pi m_W^4}\,, \tag{33}$$

$$\Gamma(\Delta^{\pm\pm} \to \Delta^{\pm\pm\pm}\pi^\mp) = \frac{3g^4 \Delta m^3 f_\pi^2}{32\pi m_W^4}\,, \tag{34}$$

where the decay constant of π meson $f_\pi = 131$ MeV. It is easy to check that the cascade decay width of $\Delta^{\pm\pm}$ into off-shell W boson is much larger than that into π meson for $|\Delta m| \gtrsim 1$ GeV.

The total width of $\Delta^{\pm\pm\pm}$ can thus be expressed as

$$\begin{aligned}\Gamma_{\Delta^{\pm\pm}} = {} & \Gamma(\Delta^{\pm\pm} \to \ell_i^\pm \ell_j^\pm) + \Gamma(\Delta^{\pm\pm} \to W^\pm W^\pm) \\ & + \theta(-\Delta m) \\ & \left[\Gamma(\Delta^{\pm\pm} \to \Delta^\pm W^{\pm *}) + \Gamma(\Delta^{\pm\pm} \to \Delta^\pm \pi^\pm)\right] \\ & + \theta(\Delta m) \\ & \left[\Gamma(\Delta^{\pm\pm} \to \Delta^{\pm\pm\pm}W^{\mp *}) + \Gamma(\Delta^{\pm\pm} \to \Delta^{\pm\pm\pm}\pi^\mp)\right],\end{aligned} \tag{35}$$

where the Heviside function $\theta(x) = 1$ for $x > 0$ and 0 for $x < 0$. For $\Delta m = 0$, only the first two terms contribute.

These three decay modes of $\Delta^{\pm\pm}$ compete with each other controlled by the quadruplet VEV v_Δ and the mass splitting Δm. To evaluate the fraction of the cascade decays, we depict the total width and decay branching ratios of $\Delta^{\pm\pm}$ for $\Delta m \leq 0$ and the NH in Fig. 4. For $\Delta m \geq 0$ and/or the IH, we can get similar results. The branching ratio of cascade decays increases with $|\Delta m|$. For $\Delta m = -1$ GeV (-10 GeV), it

is larger than 0.1 (0.8) in the range 10^{-5} GeV $\lesssim v_\Delta \lesssim 10^{-4}$ GeV ($10^{-6.5}$ GeV $\lesssim v_\Delta \lesssim 10^{-2.5}$ GeV), as shown in the right panel. Given the total width in the left panel, the proper decay length $c\tau_{\Delta^{\pm\pm}} = \hbar c/\Gamma_{\Delta^{\pm\pm}}$ can be easily obtained and is smaller than 0.1 mm for 300 GeV $\leq m_{\Delta^{\pm\pm}} \leq$ 1000 GeV, which ensures the validity of prompt search of $\Delta^{\pm\pm}$ at pp colliders.

Triply charged Higgs boson $\Delta^{\pm\pm\pm}$ can decay into $W\ell_i^\pm\ell_j^\pm$ and $W^\pm W^\pm W^\pm$ if kinetically allowed. The partial widths of three-body decays through an off-shell $\Delta^{\pm\pm}$ are

$$\begin{aligned}
&\Gamma(\Delta^{\pm\pm\pm} \to W^\pm \ell_i^\pm \ell_j^\pm) \\
&\quad = \frac{g^2 m_{\Delta^{\pm\pm\pm}}^3 |h_{ij}|^2}{768\pi^3 m_W^2 (1+\delta_{ij})} \int_0^{(m_{\Delta^{\pm\pm\pm}} - m_W)^2} ds F(s)\ , \\
&\Gamma(\Delta^{\pm\pm\pm} \to W^\pm W^\pm W^\pm) \\
&\quad = \frac{3 g^6 v_\Delta^2 m_{\Delta^{\pm\pm\pm}}^5}{4096\pi^3 m_W^6} \int_{4m_W^2}^{(m_{\Delta^{\pm\pm\pm}} - m_W)^2} \int_{t_{\min}}^{t_{\max}} dt ds G(s,t)
\end{aligned} \tag{36}$$

with

$$\begin{aligned}
F(s) &= \frac{m_W^2}{m_{\Delta^{\pm\pm\pm}}^4}\left[6(-2-2r_s+r_W+1/r_W(1-r_s)^2)\right] \\
&\quad D(s) r_s \lambda(1, r_s, r_W)^{1/2}, \qquad (37) \\
G(s,t) &= \frac{1}{m_{\Delta^{\pm\pm\pm}}^4} \\
&\quad \Big[\left[24 r_W(-2-2r_s+r_W+1/r_W(1-r_s)^2)\right] D(s) \\
&\quad \times (2r_W^2 + 1/4(r_s-2r_W)^2) \\
&\quad + 48[(1-r_s)(1-r_t) \\
&\quad - (1/2 r_W r_s + 1/2 r_W r_t + 5/2 r_W - 3/2 r_W^2)] E(s,t) \\
&\quad \times [3r_W^2 + 1/4(r_s-4r_W)(r_t-4r_W)]\Big] \qquad (38) \\
t_{\max} &= \frac{1}{4s}[(m_{\Delta^{+++}}^2 - m_W^2)^2 - (\lambda(s, m_W^2, m_W^2)^{\frac{1}{2}} \\
&\quad - \lambda(m_{\Delta^{+++}}^2, s, m_W^2)^{\frac{1}{2}})^2] \qquad (39) \\
t_{\min} &= \frac{1}{4s}[(m_{\Delta^{+++}}^2 - m_W^2)^2 - (\lambda(s, m_W^2, m_W^2)^{\frac{1}{2}} \\
&\quad + \lambda(m_{\Delta^{+++}}^2, s, m_W^2)^{\frac{1}{2}})^2]. \qquad (40)
\end{aligned}$$

and

$$D(s) = \frac{1}{(r_s - (1+\Delta m/m_{\Delta^{\pm\pm\pm}})^2)^2 + (1+\Delta m/m_{\Delta^{\pm\pm\pm}})^2 \Gamma_{\Delta^{\pm\pm}}^2/m_{\Delta^{\pm\pm\pm}}^2}\ , \tag{41}$$

$$E(s,t) = \frac{1}{(r_s - (1+\Delta m/m_{\Delta^{\pm\pm\pm}})^2)(r_t - (1+\Delta m/m_{\Delta^{\pm\pm\pm}})^2) + (1+\Delta m/m_{\Delta^{\pm\pm\pm}})^2 \Gamma_{\Delta^{\pm\pm}}^2/m_{\Delta^{\pm\pm\pm}}^2}\ . \tag{42}$$

Here, s, t denote the invariant mass of the W boson pair from the decay of $\Delta^{\pm\pm}$, $r_s \equiv s/m_{\Delta^{\pm\pm\pm}}^2$, $r_t \equiv t/m_{\Delta^{\pm\pm\pm}}^2$, $r_W \equiv m_W^2/m_{\Delta^{\pm\pm\pm}}^2$, and $\lambda(x,y,z) \equiv (x-y-z)^2 - 4yz$. In the limit of $m_W/m_{\Delta^{\pm\pm\pm}} \to 0$, the above integrations over $F(s)$ and $G(s,t)$ are equal to 1. It is noted that the total width $\Gamma_{\Delta^{\pm\pm}} \lesssim 0.01$ GeV for 10^{-9} GeV $\leq v_\Delta \leq 1$ GeV (see Fig. 4), which has negligible effect on the three-body decay widths.

We can see immediately that different from the decays of $\Delta^{\pm\pm} \to \ell_i^\pm \ell_j^\pm, W^\pm W^\pm$, the three-body decays of $\Delta^{\pm\pm\pm}$ in Eq. (36) depend on the mass splitting Δm. To estimate its impact, we introduce

$$\begin{aligned}
\delta\Gamma_{W\ell\ell} &= (\Gamma_{W\ell\ell} - \Gamma^0_{W\ell\ell})/\Gamma^0_{W\ell\ell}, \\
\delta\Gamma_{WWW} &= (\Gamma_{WWW} - \Gamma^0_{WWW})/\Gamma^0_{WWW},
\end{aligned} \tag{43}$$

where $\Gamma_{W\ell\ell} = \sum_{i,j}\Gamma(\Delta^{\pm\pm\pm} \to W^\pm \ell_i^\pm \ell_j^\pm)$ and $\Gamma_{WWW} = \Gamma(\Delta^{\pm\pm\pm} \to W^\pm W^\pm W^\pm)$ and $\Gamma^0_{W\ell\ell}$ and Γ^0_{WWW} are the corresponding values with $\Delta m = 0$. In Fig. 5, the values of $\delta\Gamma_{W\ell\ell}$ and $\delta\Gamma_{WWW}$ are shown. We find that both $\delta\Gamma_{\ell\ell W}$ and $\delta\Gamma_{WWW}$ are negligible for $|\Delta m| = 1$ GeV and increase to 10% − 25% for $|\Delta m| = 10$ GeV in the mass range 300 GeV $\leq m_{\Delta^{\pm\pm\pm}} \leq$ 1000 GeV.

The interplay between the decays $\Delta^{\pm\pm\pm} \to W^\pm \ell_i^\pm \ell_j^\pm$ and $\Delta^{\pm\pm\pm} \to W^\pm W^\pm W^\pm$ is the similar to that for $\Delta^{\pm\pm}$ in two-body decays. Therefore, we need to include the cascade decays of $\Delta^{\pm\pm\pm}$ with $\Delta^{\pm\pm}$ being on shell in the medium v_Δ region for $\Delta m < 0$ with the widths being approximately given by

$$\Gamma(\Delta^{\pm\pm\pm} \to \Delta^{\pm\pm} W^{\pm *}) = -\frac{9 g^4 \Delta m^5}{160\pi^3 m_W^4}\ , \tag{44}$$

$$\Gamma(\Delta^{\pm\pm\pm} \to \Delta^{\pm\pm}\pi^\pm) = -\frac{3 g^4 \Delta m^3 f_\pi^2}{32\pi m_W^4}. \tag{45}$$

For $\Delta m > 0$, the cascade decay of $\Delta^{\pm\pm\pm}$ is kinetically forbidden. Hence, the total width of $\Delta^{\pm\pm\pm}$ is expressed as

$$\begin{aligned}
\Gamma_{\Delta^{\pm\pm\pm}} &= \Gamma(\Delta^{\pm\pm\pm} \to W^+ \ell_i^\pm \ell_j^\pm) \\
&\quad + \Gamma(\Delta^{\pm\pm\pm} \to W^\pm W^\pm W^\pm) \\
&\quad + \theta(-\Delta m) \\
&\quad \Big[\Gamma(\Delta^{\pm\pm\pm} \to \Delta^{\pm\pm} W^{\pm *}) \\
&\quad + \Gamma(\Delta^{\pm\pm\pm} \to \Delta^{\pm\pm}\pi^\pm)\Big].
\end{aligned} \tag{46}$$

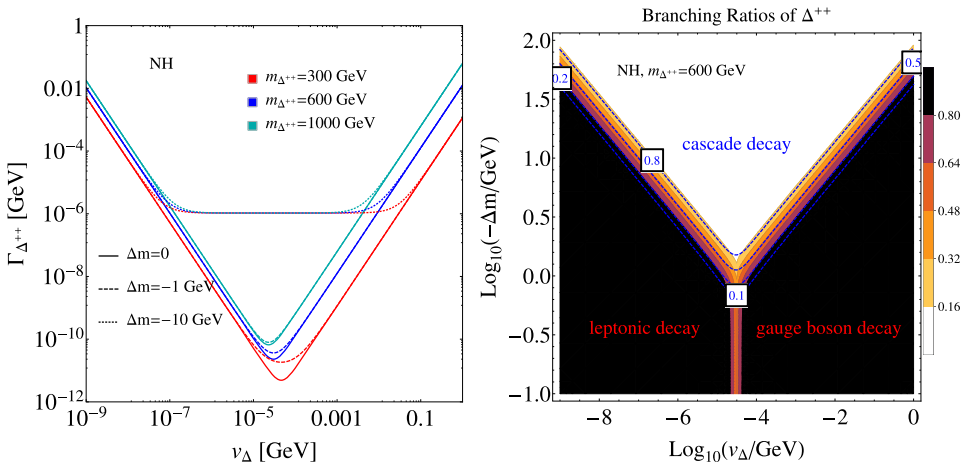

Fig. 4 Left: total decay width of $\Delta^{\pm\pm}$ defined in Eq. (35) as a function of the quadruplet VEV v_Δ for $m_{\Delta^{\pm\pm}} = 300, 600, 900$ GeV for the NH. The solid, dashed, dotted curves correspond to $\Delta m = 0, -1, -10$ GeV, respectively. Right: decay branching ratios of $\Delta^{\pm\pm}$ in the plane of $\log_{10}(v_\Delta/\text{GeV})$ and $\log_{10}(-\Delta m/\text{GeV})$ for $m_{\Delta^{\pm\pm}} = 600$ GeV and the NH. The shaded regions represent the branching ratios in the leptonic decay and gauge boson decay channels for $v_\Delta \lesssim 10^{-4.5}$ GeV and $v_\Delta \gtrsim 10^{-4.5}$ GeV, respectively. The blue curves denote the branching ratio in the cascade decay channel

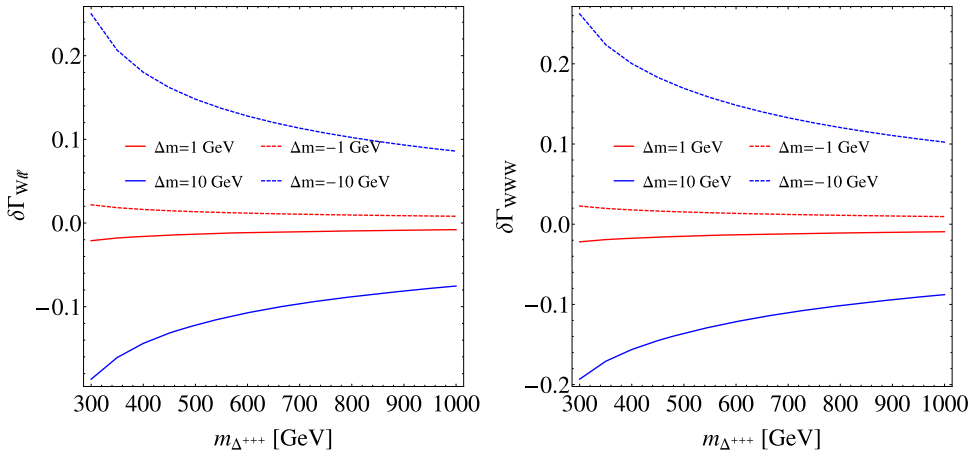

Fig. 5 Impact of Δm on the partial decay widths of $\Delta^{\pm\pm\pm}$ into $W^\pm \ell_i^\pm \ell_j^\pm$ and $W^\pm W^\pm W^\pm$ in the left and right panels, respectively. Benchmark values of $|\Delta m| = 1, 10$ GeV are considered

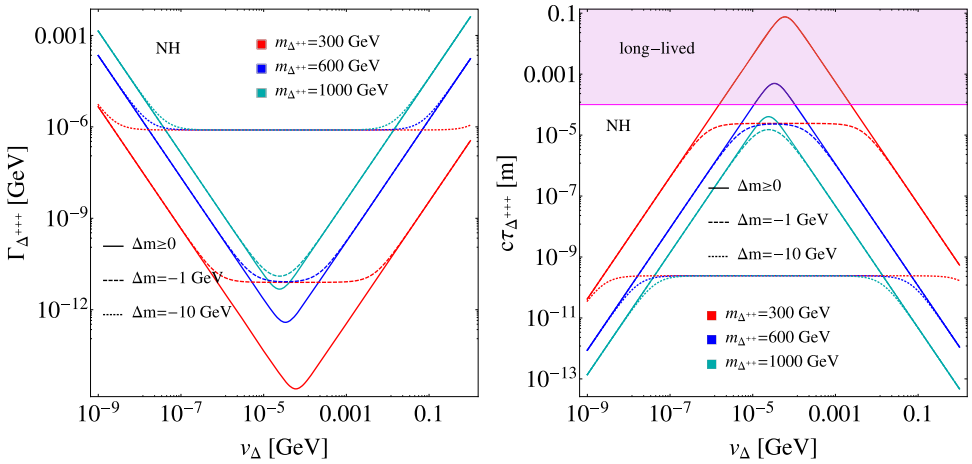

Fig. 6 Total decay width (let panel) and proper decay length (right panel) of $\Delta^{\pm\pm}$ defined in Eq. (35) as a function of the quadruplet VEV v_Δ for $m_{\Delta^{\pm\pm}} = 300, 600, 1000$ GeV with the NH. The solid, dashed, dotted curves correspond to $\Delta m = 0, -1, -10$ GeV, respectively. In the magneta shaded region, $c\tau_{\Delta^{\pm\pm\pm}} \geq 0.1$ mm, $\Delta^{\pm\pm\pm}$ is long-lived

The total width and proper decay width of $\Delta^{\pm\pm\pm}$ are depicted in Fig. 6. It is interesting to observe that since the three-body decay widths of $\Delta^{\pm\pm}$ are much smaller than the two-body decay widths of $\Delta^{\pm\pm}$, the cascade decay dominates in the medium v_Δ region for $\Delta m < 0$ even with $\Delta m = -1$ GeV. For $\Delta m > 0$, the cascade decays are not allowed and the dependence of three-body decays on Δm is not shown explicitly for simplicity. In the left panel of Fig. 6, the total width can be as small as 10^{-15} GeV so that the proper decay length can reach 0.1 mm $\sim$ 0.1 m – the region that is inappropriate for prompt search [71], as shown in the right panel. For $\Delta m < 0$, however, the proper decay length is large enough for the prompt search with the contribution of cascade decays added.

It is important to emphasize that although the partial widths of three-body decays and cascade decays depend on the mass splitting Δm, the decay branching ratios of $\Delta^{\pm\pm\pm}$ are almost independent of Δm. For $\Delta m > 0$, the Δm dependence of the partial widths cancels in the branching ratios of $\Delta^{\pm\pm\pm}$, resulting in a modification smaller than 1.7% for $\Delta m = 10$ GeV. For $\Delta m < 0$, the cancellation is similar in the low and high v_Δ regions as that for $\Delta m > 0$. In the medium v_Δ region, the cascade decay dominates over the three-body decays, which ensures that the branching ratio is independent of Δm.

5 Collider analysis

In this section, we will perform collider studies of triply charged Higgs bosons at pp colliders. Given the couplings of $\Delta^{\pm\pm}$ to charged leptons and W bosons, we have the decay channels: for the DYZ and PF processes $\Delta^{+++}\Delta^{---} \to (\ell^+\ell^+W^+)(\ell^-\ell^-W^-)$, $(\ell^\pm\ell^\pm W^\pm)(W^\mp W^\mp W^\mp)$, and $(W^+W^+W^+)(W^-W^-W^-)$; for the DYW process $\Delta^{\pm\pm\pm}\Delta^{\mp\mp} \to (\ell^\pm\ell^\pm W^\pm)(\ell^\mp\ell^\mp)$, $(\ell^\pm\ell^\pm W^\pm)(W^\mp W^\mp)$, $(W^\pm W^\pm W^\pm)(\ell^\mp\ell^\mp)$, and $(W^\pm W^\pm W^\pm)(W^\mp W^\mp)$, where $\ell \equiv e, \mu, \tau$. If one or more on-shell W bosons decay into leptons, we can always achieve the inclusive final state with at least three same-sign leptons. We also include the cascade decays for $|\Delta m| \lesssim 30$ GeV. In case of $\Delta m > 0$, $\Delta^{\pm\pm} \to \Delta^{\pm\pm\pm}W^{\mp *}$, while in case of $\Delta m < 0$, $\Delta^{\pm\pm\pm} \to \Delta^{\pm\pm}W^{\pm *}$ and $\Delta^{\pm\pm} \to \Delta^{\pm}W^{\pm *}$. In the latter case, the momenta of leptons and jets from off-shell W bosons are limited by the mass splitting, so that they are unlikely to be detected [54–56]. To this end, we will assume that $\Delta m \geq 0$ and the efficiency of $\Delta^{\pm\pm} \to (\Delta^{\pm\pm\pm} \to X)(W^{\mp *} \to \ell\nu/jj)$ is the same as that of $\Delta^{\pm\pm\pm} \to X$.

The SM backgrounds are those with at least three same-sign charged leptons in the final states. In previous studies, the backgrounds $t\bar{t}W$ [37–39,72,73], $t\bar{t}Z$ [37,73], $t\bar{t}t\bar{t}$ [37,72,73], $t\bar{t}b\bar{b}$ [37,72], $t\bar{t}h$ [73], WWZ [73], WZZ [73] and ZZZ [73] were considered. In Ref. [39], the backgrounds WZ and ZZ were discussed with charge misidentification of leptons taken into account.

In our study, we consider the backgrounds with at least two same-sign leptons at parton level and the third same-sign lepton could come from heavy-flavor hadron decays or charge misidentification. Besides, the $t\bar{t}$ background is also taken into account, since its cross section is huge. The set of backgrounds can be read off from the experimental searches for final states with same-sign leptons or multiple leptons [40,74,75], which are classified into $t\bar{t}$ production in association with a boson ($t\bar{t}W$, $t\bar{t}Z/\gamma^*$, $t\bar{t}h$ with h being the SM Higgs boson), multi-top production ($t\bar{t}$, $t\bar{t}t/\bar{t}$, $t\bar{t}t\bar{t}$), multi-boson production (WZ, $Z/\gamma^*\,WWW$, WWZ, WZZ, ZZZ, $WW\gamma^*$, $WZ\gamma^*$) and rare processes ($t\bar{t}b\bar{b}$, tWZ, $t/\bar{t}Zq$) with q denoting one of quarks except $t/\bar{t}$.

The comments on the backgrounds are made as follows. Backgrounds with an off-shell photon, such as $t\bar{t}\gamma^*$, are not generated since their contributions are expected to be reduced significantly after imposing the lower cuts on the invariant mass of opposite-sign same-flavor leptons in Cut-3 (see the definition below) as compared to the corresponding backgrounds with an on-shell Z boson. The backgrounds $t\bar{t}h, h \to b\bar{b}, WW^*$ are not considered since their cross sections are much smaller than those of $t\bar{t}b\bar{b}$, $t\bar{t}W$. For the background $t\bar{t}Z$, we only consider the decay $Z \to \ell^+\ell^-$ and neglect $Z \to q\bar{q}$ since the latter cross section is much smaller as compared to $t\bar{t}jj$ and $t\bar{t}b\bar{b}$. The tri-top production $t\bar{t}t/\bar{t}$ [76] with a much smaller cross section than that of $t\bar{t}W$ [77] can be neglected.

The charge misidentification probability is about $10^{-5} \sim 10^{-3}$ for electrons (ϵ_e) due to bremsstrahlung interactions with the inner detector material and negligible for muons at the 13 TeV LHC [74,75,78,79]. At a 100 TeV pp collider, we assume a conservative and uniform rate $\epsilon_e = 10^{-3}$ [80]. The charge-misidentified backgrounds are obtained from reweighting the background by the charge misidentification probabilities [78], see Table 1. Backgrounds with a non-prompt lepton may fake the signal, which originates from hadron decays or in photon conversions as well as hadrons misidentified as leptons. It is shown at the 13 TeV LHC that the non-prompt leptons mainly come from heavy-flavor hadron decays in events containing top quark, W boson or Z boson [40]. Besides, the probability of jet faking lepton can also be reduced with the cut on missing energy [72,73,75,79,81], i.e., Cut-5 below[7]. Therefore, we will only consider non-prompt leptons from heavy-flavor hadron decays at pp colliders in this study.

We generate parton-level signal and background events at $\sqrt{s} = 100$ TeV using `MG5_aMC@NLO v2.6.5` [64], which

[7] Non-prompt leptons from jet faking can be distinguished from the prompt leptons in W/Z decays with delicated isolation variables [78].

Table 1 The charge misidentification probabilities of backgrounds with $e^+e^+/e^+\mu^+/\mu^+\mu^+$ and one electron e^- or two electrons e^-e^-. The same probabilities can be obtained for the charge-conjugated combinations

	e^-	e^-e^-
e^+e^+	ϵ_e	$4\epsilon_e$
$e^+\mu^+$	ϵ_e	$3\epsilon_e$
$\mu^+\mu^+$	ϵ_e	$2\epsilon_e$

are passed to `Pythia8` [82] for possible sequential decays, parton shower and hadronization. The default factorization and renormalization scales are used. The backgrounds WZ and $t\bar{t}$ are matched upto two additional jets [31], $t\bar{t}t\bar{t}$, $t\bar{t}b\bar{b}$ and $t/\bar{t}Zq$ are generated without additional partons for simplicity, while the other backgrounds are matched to additional one jet.

The next-leading-order QCD overall K-factors of the background processes are available at the LHC colliding energy $\sqrt{s} = 14$ TeV ranging from 1.2 to 2.0 [83–94]. As an estimate, we apply these K-factors to the corresponding processes at $\sqrt{s} = 100$ TeV [80]. The detector response is simulated using `Delphes` [95] with the built-in baseline FCC-hh detector configuration. The probability of one b quark to be identified as b-jet is $[1 - p_T/(20\,\text{TeV})] \cdot 85\%$ and the mis-taggig efficiencies for light-flavor quarks and c-quark wrongly identified as b-jets are $[1 - p_T/(20\,\text{TeV})] \cdot 1\%$ and $[1 - p_T/(20\,\text{TeV})] \cdot 5\%$ in the central region ($|\eta| < 2.5$) [96].

In order to identify objects, we impose the following criteria [80,97]

$$p_{T,e/\mu} > 20\ \text{GeV}, \quad p_{T,j/b} > 30\ \text{GeV}, \quad |\eta_{e/\mu/j/b}| < 6, \tag{47}$$

where j and b denote the light-flavor jets and b-tagged jet, respectively. The lepton candidates are isolated within a cone of radius of 0.3, and the jet candidates are clustered with the anti-k_t algorithm [98] and a radius parameter of 0.4 implemented in the `FastJet` package [99].

Events are then selected with a series of cuts. It is demanded the angular separation between any two reconstructed objects satisfies[8] $\Delta R \equiv \sqrt{(\Delta\eta)^2 + (\Delta\phi)^2} > 0.3$ [97] (Cut-1), which can help to reject leptons from the decay of a b-hadron or c-hadron [100]. Three or more charged leptons are required with the p_T of the leading, sub-leading and sub-sub-leading leptons larger than 50 GeV, 35 GeV and 25 GeV, respectively and at least two of them have the same charge (Cut-2), where ℓ_1. To reduce backgrounds from Drell-Yan processes and Z boson decays, events with opposite-sign same-flavor lepton pairs or same-sign electron pairs with the invariant mass below 12 GeV or within the mass window of 15 GeV around the Z boson mass are rejected [74,75] (Cut-3). For the signal processes, the final states can be $\ell^+\ell^+\ell^+\ell^-\ell^-(\ell^-/jj)E_T^{\text{miss}}$, $\ell^+\ell^+\ell^+\ell^- jj(\ell^-/jj)E_T^{\text{miss}}$, $\ell^+\ell^+\ell^+ jjjj(\ell^-/jj)E_T^{\text{miss}}$, and the charge-conjugated ones. Therefore, we further impose the following selection cuts:

- exactly three same-sign leptons are required (Cut-4);
- missing transverse momentum $E_T^{\text{miss}} > 50$ GeV (Cut-5);
- b-tagged jets are vetoed (Cut-6);

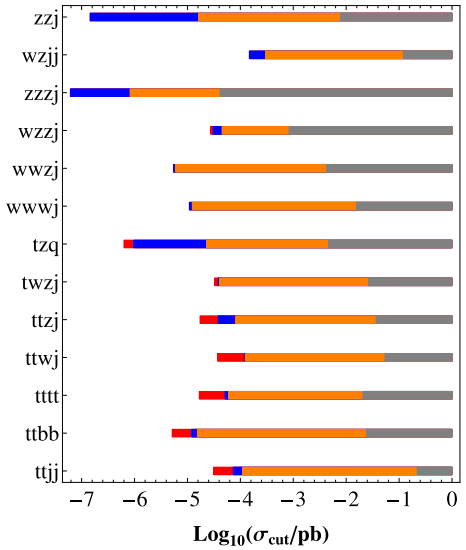

Fig. 7 Cut flow of the background processes. The left endpoints of the gray, orange, blue and red bands correspond to the cross sections after Cut-3 to Cut-6, respectively

It is noted that experimental search for signals in final state with SS3L signature and at least one b-tagged jet has be performed [40], which is typically different from our context. Cuts on objects other than the three same-sign leptons can also be imposed. For example, one can require the sum of the residual lepton number and jet number to be larger than 2. In this paper, we however only consider Cut-1 to Cut-6 for an easier comparison with previous studies.

It is straightforward to obtain the cut flow of cross sections after the selection cuts. In Fig. 7, cross sections of the background processes after Cut-3 to Cut-6 are depicted, where the left endpoints of the gray, orange, blue and red bands correspond to the cross sections after Cut-3 to Cut-6, respectively. Assuming that the cross section after Cut-i is σ_{cut}^i and the corresponding cut efficiency is $\epsilon_i = \sigma_{\text{cut}}^i/\sigma_0$ with σ_0 being the background cross section before any cut, one obtains the relation

$$\log_{10}\sigma_{\text{cut}}^i - \log_{10}\sigma_{\text{cut}}^{i-1} = \log_{10}\frac{\epsilon_i}{\epsilon_{i-1}}\,. \tag{48}$$

[8] $\Delta\eta$ and $\Delta\phi$ denote the pseudo-rapidity and azimuthal angle difference between any two reconstructed objects.

Therefore, the length of each colored band characterizes the cut efficiency of an individual cut. The total cross section of backgrounds ~ 0.34 fb after selection cuts is dominated by WZ, $t\bar{t}W$, $t\bar{t}$, $t\bar{t}Z$, while the backgrounds $t\bar{t}t\bar{t}$ and $t\bar{t}b\bar{b}$ are less important [72]. We can see that the background ZZ becomes negligible after imposing selection cut on the missing transverse momentum.

To evaluate the signal significance, we use [101]

$$\mathcal{Z} = \sqrt{2\left[(n_s + n_b)\log\frac{n_s + n_b}{n_b} - n_s\right]}\,, \tag{49}$$

where n_s and n_b denote the numbers of signal and background events after selection cuts. This formula is valid even for $n_b \ll n_s$ [101]. The discovery prospects of individual signal process are depicted in Fig. 8. The solid, dashed and dotted curves correspond to the required integrated luminosities to reach 5σ discovery for $\Delta m = 0$, 1 GeV and 10 GeV, respectively. Doubly and triply charged Higgs bosons decay into on-shell leptons and gauge bosons in the low and high v_Δ regions, respectively, alongside with a smooth transition in the medium v_Δ region due to the cascade decay of $\Delta^{\pm\pm}$. It is apparent that a larger integrated luminosity is required for $v_\Delta \gtrsim 10^{-3}$ GeV than for $v_\Delta \lesssim 10^{-5}$ GeV since in the latter case $\Delta^{\pm\pm(\pm)}$ mainly decays into W bosons and the signal cross section is dissipated by the decays of W bosons. We can see that with the integrated luminosity of about 0.1 (10), 1 (25), 10 fb^{-1} (400 fb^{-1}), the triply charged Higgs boson with mass being 300, 600, 1000 GeV can be discovered in the DYZ process for $v_\Delta \lesssim 10^{-5}$ GeV ($v_\Delta \gtrsim 10^{-3}$ GeV). The integrated luminosity required to reach 5σ discovery in the DYW process are larger than that in the DYZ process except for the case with $m_{\Delta^{\pm\pm\pm}} = 300$ GeV and $v_\Delta \gtrsim 10^{-3}$ GeV, since there are more combinations of decays in the DYZ process and the phase space for $m_{\Delta^{\pm\pm\pm}} = 300$ GeV and $v_\Delta \gtrsim 10^{-3}$ GeV in the DYZ process is more severely suppressed. For the same reason, the PF cross section for $m_{\Delta^{\pm\pm\pm}} = 300$ GeV is close to that for $m_{\Delta^{\pm\pm\pm}} = 600$ GeV in the range of $v_\Delta \gtrsim 10^{-3}$ GeV.

We can also find that the DYW process is more sensitive to the cascade decay $\Delta^{\pm\pm} \to \Delta^{\pm\pm\pm}W^{\mp *}$ as compared to the DYZ and PF processes. In the DYZ and PF processes, the production of both $\Delta^{+++}\Delta^{---}$ and $\Delta^{++}\Delta^{--}$ with the decays $\Delta^{\pm\pm} \to \Delta^{\pm\pm\pm}W^{\mp *}$ and $\Delta^{\pm\pm\pm} \to \ell^\pm\ell^\pm W^\pm$, $W^\pm W^\pm W^\pm$ are considered. Since the production cross section of $\Delta^{++}\Delta^{--}$ are about 20% of $\Delta^{+++}\Delta^{---}$, the required luminosities to reach 5σ discovery are lowered slightly for $\Delta m = 10$ GeV as compared to that for $\Delta m = 0$ in the medium v_Δ region. For the DYW process, we consider the production of $\Delta^{\pm\pm\pm}\Delta^{\mp\mp}$ with the decays $\Delta^{\pm\pm} \to \Delta^{\pm\pm\pm}W^{\mp *}$, $\ell^\pm\ell^\pm$, $W^\pm W^\pm$ and $\Delta^{\pm\pm\pm} \to \ell^\pm\ell^\pm W^\pm$, $W^\pm W^\pm W^\pm$. In the medium v_Δ region the sensitivity is remarkably improved due to more combinations of decays, except for $m_{\Delta^{\pm\pm\pm}} = 300$ GeV and $v_\Delta \gtrsim 10^{-3}$ GeV when the decay $\Delta^{\pm\pm\pm} \to W^\pm W^\pm W^\pm$ is suppressed kinematically.

The discovery prospects after combining the signals in the DYW, DYZ and PF processes are shown in Fig. 9. With the integrated luminosity of about 100 fb^{-1}, the triply charged Higgs boson with mass below 1000 GeV can be discovered. Besides, the required integrated luminosity to reach 5σ in the region of $v_\Delta \lesssim 10^{-5}$ GeV for the IH is smaller than that for the NH. This is because the coupling of $\Delta^{\pm\pm}$ to the electron pair for the IH is larger. For $v_\Delta \gtrsim 10^{-3}$ GeV, the sensitivities for the NH and IH are are the same since $\Delta^{\pm\pm(\pm)}$ mainly decays into $W^\pm W^\pm(W^\pm)$, which is independent of the neutrino mass hierarchy. Below, we will concentrate on the sensitivities for the NH.

To illustrate the dependence of 5σ contours on the mass splitting Δm, we show the 5σ discovery reach in the plane of $\log_{10}(\mathcal{L}/\text{fb}^{-1})$ and Δm in Fig. 10 with two benchmark values $v_\Delta = 10^{-6}$ GeV and 5×10^{-3} GeV, which ensure $\text{Br}(\Delta^{\pm\pm\pm} \to \ell^\pm\ell^\pm W^\pm) = 1$ and $\text{Br}(\Delta^{\pm\pm\pm} \to W^\pm W^\pm W^\pm) = 1$ for $\Delta m \geq 0$, respectively. Moreover, from the right panel of Fig. 6, the proper decay lengths for $v_\Delta = 10^{-6}$ GeV and 5×10^{-3} GeV are both larger than 0.1 mm, which ensures the validity of prompt search. We can see that the integrated luminosities to reach 5σ discovery decreases with Δm for $0 < \Delta m \lesssim 10$ GeV (15 GeV) for $v_\Delta = 10^{-6}$ GeV (5×10^{-3} GeV) as shown in Fig. 10.

Finally, the sensitivities at the FCC-hh and the LHC are compared. The latter one has been investigated in Refs. [38,39] with the above benchmark values of v_Δ being chosen. Different from the significance formula in Eq. (49), they used $n_s/\sqrt{n_s + n_b}$ to quantify the significance and found that at 5σ level $m_{\Delta^{\pm\pm\pm}} \lesssim 950$ GeV can be reached at the LHC with the integrated luminosity of 3 ab^{-1} for $v_\Delta = 10^{-6}$ GeV, while it is reduced to $m_{\Delta^{\pm\pm\pm}} \lesssim 600$ GeV for $v_\Delta = 5 \times 10^{-3}$ GeV. However, it is known [101] that $n_s/\sqrt{n_s + n_b}$ is a good approximation of the significance $\mathcal{Z}$ in Eq. (49) only if $n_s \ll n_b$. In our case, n_s and n_b can be comparable. As a result, we find that $n_s/\sqrt{n_s + n_b}$ underestimates the significance by several times. As a result, the integrated luminosities required to reach $\mathcal{Z} = 5$ can be smaller than that with $n_s/\sqrt{n_s + n_b} = 5$ by one or two orders. To be more concrete, in Table III of Ref. [39], the signal cross section with $(m_{\Delta^{\pm\pm\pm}}, \Delta m, v_\Delta) = (400\text{ GeV}, 0, 10^{-6}\text{ GeV})$ for the NH is 1.19×10^{-3} pb and the total background cross section is 1.21×10^{-3} pb. From the left panel of Fig. 22 of Ref. [39], we can infer that the signal cross section with $(m_{\Delta^{\pm\pm\pm}}, \Delta m, v_\Delta) = (600\text{ GeV}, 0, 10^{-6}\text{ GeV})$ for the NH is 2.66×10^{-4} pb. The corresponding integrated luminosities required to satisfy $\mathcal{Z} = 5$ and $n_s/\sqrt{n_s + n_b} = 5$ are 3.2 fb^{-1} and 21.2 fb^{-1} for $m_{\Delta^{\pm\pm\pm}} = 400$ GeV, and are 23.7 fb^{-1} and 3 ab^{-1} for $m_{\Delta^{\pm\pm\pm}} = 600$ GeV.

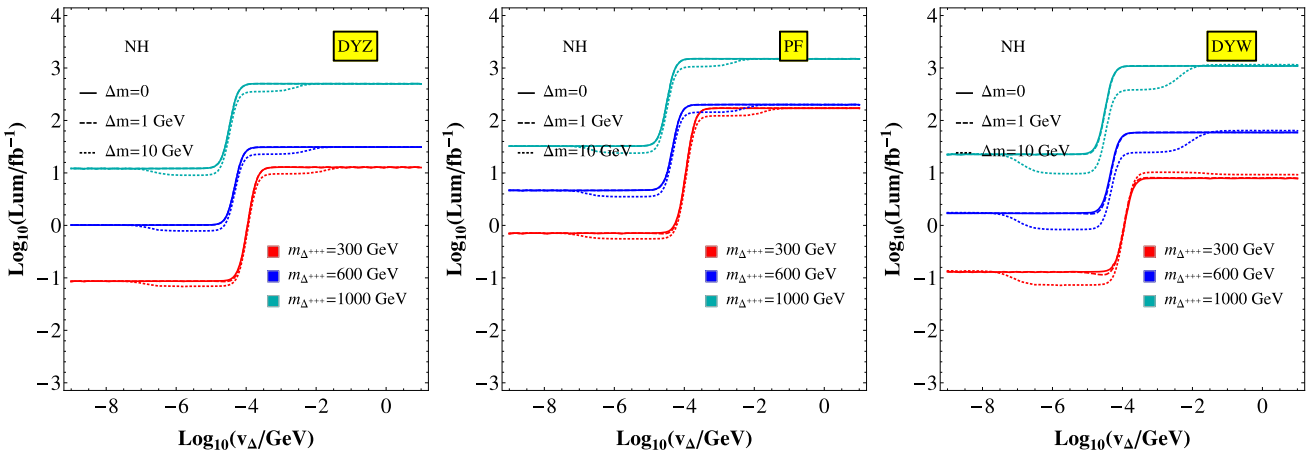

Fig. 8 5σ discovery prospects of searching for triply charged Higgs boson at a 100 TeV pp collider with SS3L signature in the DYZ, PF and DYW processes. The benchmark scenarios with $\Delta m = 0, 1, 10$ GeV and $m_{\Delta^{\pm\pm\pm}} = 300, 600, 1000$ GeV for the NH are depicted in the plane of $\log_{10}(v_\Delta/\text{GeV})$ and $\log_{10}(\mathcal{L}/\text{fb}^{-1})$

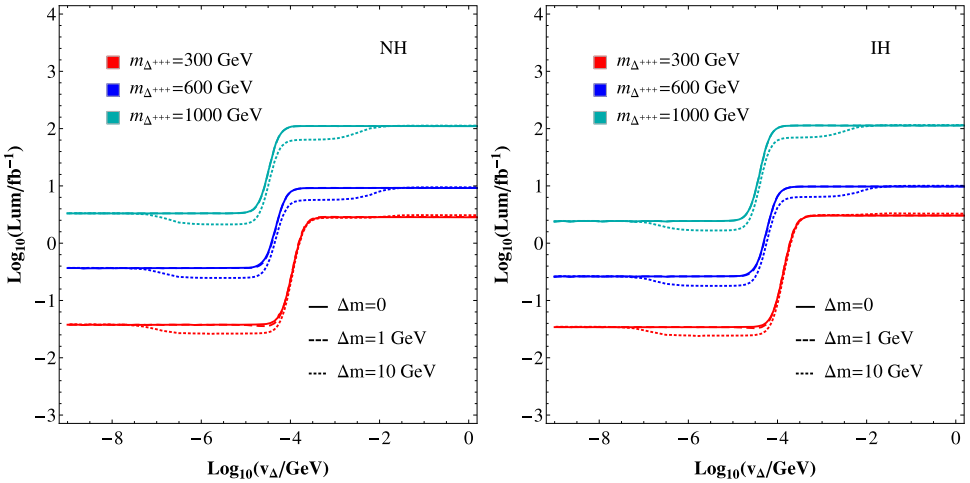

Fig. 9 5σ discovery prospects of searching for triply charged Higgs boson at a 100 TeV pp collider with SS3L signature. The benchmark scenarios with $\Delta m = 0, 1, 10$ GeV and $m_{\Delta^{\pm\pm\pm}} = 300, 600, 1000$ GeV for the NH and IH are depicted in the plane of $\log_{10}(v_\Delta/\text{GeV})$ and $\log_{10}(\mathcal{L}/\text{fb}^{-1})$

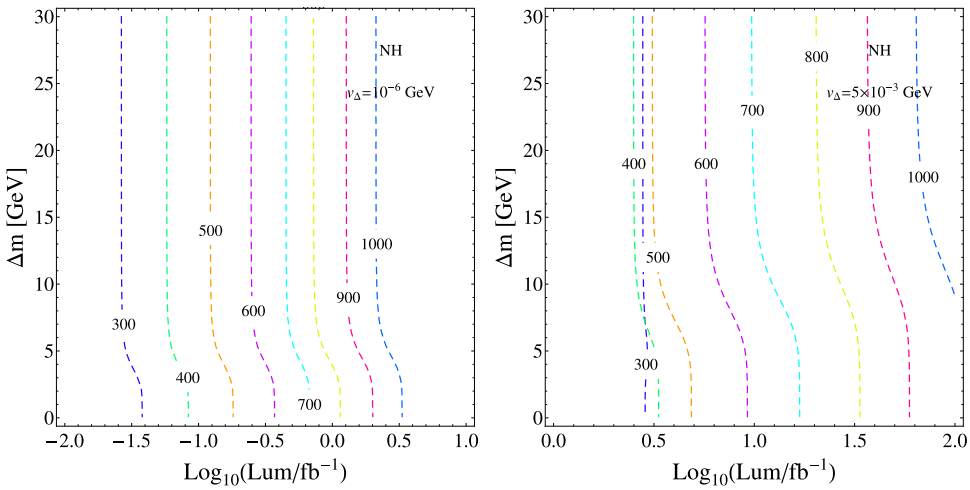

Fig. 10 5σ discovery reach in the plane of $\log_{10}(\mathcal{L}/\text{fb}^{-1})$ and Δm with two benchmark values of $v_\Delta = 10^{-6}$ GeV and 5×10^{-3} GeV in the left and right panels, respectively. The 5σ contours are labelled by the mass $m_{\Delta^{\pm\pm\pm}}$ in units of GeV

Table 2 Cross sections (in units of pb) of the backgrounds at 100/13 TeV before cuts and after cuts, which are denoted as $\sigma_0(100/13\ \text{TeV})$ and $\sigma_{\text{cut}}(100/13\ \text{TeV})$, respectively. The K-factors for each process are listed in the second column. The notation of "aE±0b" stands for $a \times 10^{\pm b}$

background	K-factor	σ_0(100 TeV)	σ_{cut}(100 TeV)	σ_0(13 TeV)	σ_{cut}(13 TeV)
ttjj	1.5	1.07E+03	3.15E-05	6.58E+01	1.94E-06
ttbb	1.77	1.07E+02	4.86E-06	1.21E+00	5.49E-08
tttt	1.21	2.39E-01	1.36E-05	7.20E-04	4.09E-08
ttwj	1.28	8.41E-01	9.04E-05	2.23E-02	2.40E-06
ttzj	1.35	1.05E+00	1.22E-05	1.41E-02	1.65E-07
twzj	1.45	7.06E-01	1.55E-05	1.44E-02	3.16E-07
tzq	1.1	4.88E-01	6.15E-07	1.13E-02	1.43E-08
wwwj	1.74	1.55E-01	1.20E-05	7.15E-03	5.53E-07
wwzj	1.98	7.27E-02	2.87E-06	2.88E-03	1.14E-07
wzzj	1.96	3.28E-02	1.73E-05	1.17E-03	6.20E-07
zzzj	1.58	2.02E-03	3.93E-08	1.18E-04	2.30E-09
wzjj	1.83	7.23E+00	1.34E-04	4.94E-01	9.14E-06
zzj	1.47	5.19E-01	1.23E-07	4.60E-02	1.09E-08

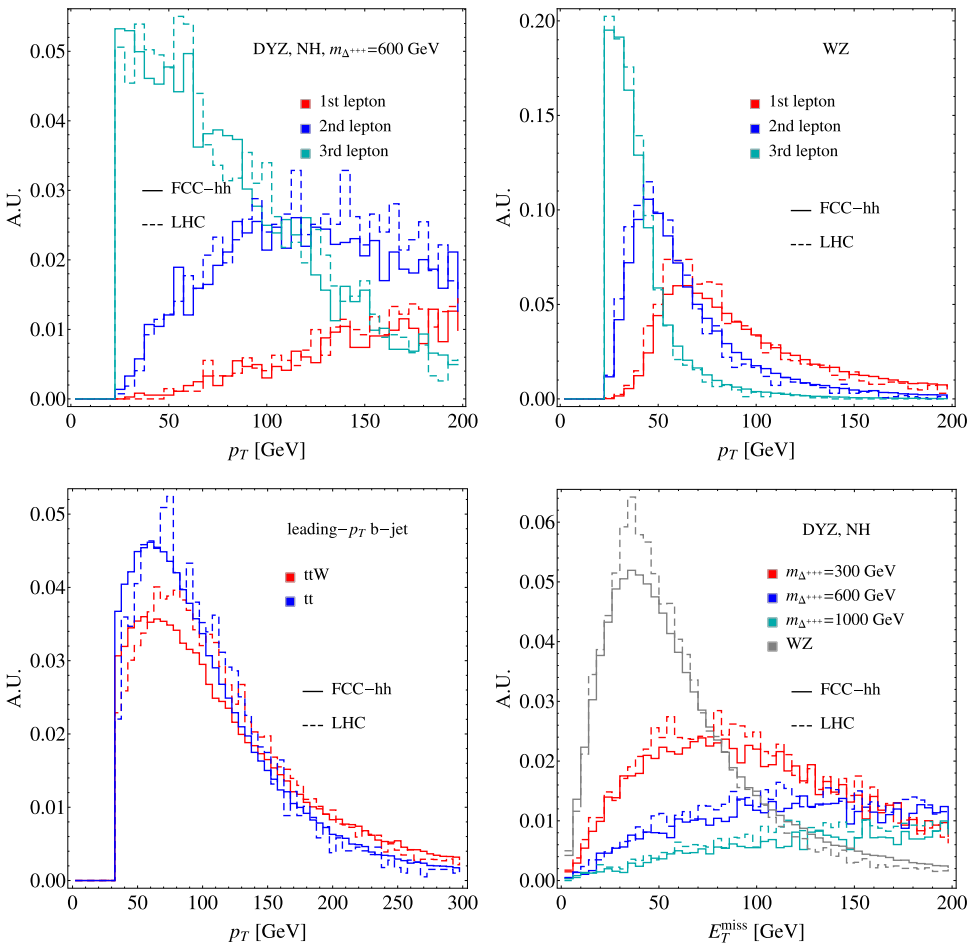

Fig. 11 The normalized distributions with an arbitrary unit (A.U.) of p_T and E_T^{miss}. Upper left: p_T for leptons in the DYZ process for the NH and $m_{\Delta^{\pm\pm\pm}} = 600$ GeV; upper right: p_T for leptons in the background WZ process; lower left: p_T for leading-p_T b-jet in the backgrounds ttW and $t\bar{t}$ processes; lower right: E_T^{miss} in the DYZ process for the NH and $m_{\Delta^{\pm\pm\pm}} = 600$ GeV and in the background WZ process. Leptons ordered by p_T are denoted by 1st, 2nd and 3rd ones

Ref. [39] present the discovery prospects of $n_s/\sqrt{n_s + n_b}$=5 with the integrated luminosities of 100 fb^{-1} and 3 ab^{-1}, which are unable to be converted into the discovery prospects of $\mathcal{Z} = 5$ with varying Δm and $m_{\Delta^{\pm\pm\pm}}$. On the other hand, we find that it is feasible to obtain the sensitivity at the LHC by projecting the result at the FCC-hh, which is obtained by the delicate detector simulation shown above. To verify this point, we compare the kinematic distributions of the signals and backgrounds at the 13 TeV LHC and FCC-hh in Figs. 11 and 12. Figure 11 displays the distributions of p_T for leptons and leading-p_T b-jet and E_T^{miss}. One can see that these distributions at the 13 TeV LHC and FCC-hh are close to each other. The most notable difference at these two colliders comes from the rapidity distributions [80], which are

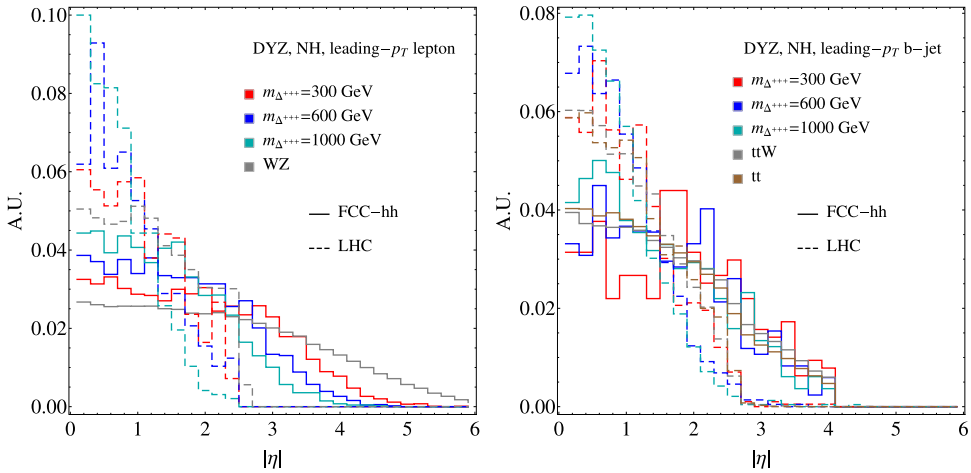

Fig. 12 The normalized distributions of the rapidity $|\eta|$ in the DYZ process for the NH and $m_{\Delta^{\pm\pm\pm}} = 300$, 600 and 1000 GeV and backgrounds. $|\eta|$ for the leading p_T lepton and b-jet for the left and right panels, respectively

shown in Fig. 12. The leptons and b-jets tend to have a larger rapidity at the FCC-hh than that at the LHC. The cut efficiencies mainly depend on the p_T and η of leptons and $E_T^{\rm miss}$[9] Therefore, if we impose the same cuts[10] at the LHC as that at the FCC-hh, the cut efficiencies at these two colliders are expected to be roughly the same. This enables us to evaluate the signal significance at the LHC without repeating the collider simulation.

In the last two columns of Table 2, we show the cross sections of background processes without any cut and after all cuts at the 13 TeV LHC as a recast of cross sections at the FCC-hh assuming the same cut efficiencies, which are denoted as $\sigma_0(13\ \text{TeV})$ and $\sigma_{\rm cut}(13\ \text{TeV})$, respectively. We obtain that the dominant backgrounds at the LHC are WZ, $t\bar{t}W$ and $t\bar{t}$. The cross section of WZ is 9.14×10^{-6} pb after cuts, which is slightly smaller than that in Ref. [39] probably owing to a larger $E_T^{\rm miss}$ cut that we have imposed. The cross section of background ZZ we obtain is smaller than that in Ref. [39] since we have further rejected events with lepton invariant mass below 12 GeV as in Cut-2. The cross section of background $t\bar{t}W$ we obtain is larger since we have considered both leptonic and hadronic decays of top quark. The signal cross section with $(m_{\Delta^{\pm\pm\pm}}, \Delta m, v_\Delta) = (400\ \text{GeV}, 0, 10^{-6}\ \text{GeV})$ for the NH is 2.2×10^{-3} pb, which is about 2 times of that in Ref. [39]. This is because we have multiplied a K-factor of 1.25 for the DY cross section. Besides, the PF process has also been included in our analysis, the cross section of which for $m_{\Delta^{\pm\pm\pm}} = 400$ GeV is comparable to that of the DYW or DYZ cross section, see Fig. 3.

Finally, we summarize constraints and discovery prospects in the plane of $m_{\Delta^{\pm\pm\pm}}$ and Δm with the banchmark values of $v_\Delta = 10^{-6}$ GeV and 5×10^{-3} GeV for the NH in Fig. 13. The 5σ contours correspond to the integrated luminosities required to satisfy $\mathcal{Z} = 5$. At the 13 TeV LHC, the regions of $\Delta m \geq 0$ and 300 GeV $\leq m_{\Delta^{\pm\pm\pm}} \leq 1000$ GeV can be discovered with the integrated luminosity of 330 fb^{-1} for $v_\Delta = 10^{-6}$ GeV, while the region of $m_{\Delta^{\pm\pm\pm}} > 800$ GeV for $v_\Delta = 5 \times 10^{-3}$ GeV is unable to be discovered even with the integrated luminosity of 3 ab^{-1}. At the FCC-hh, the regions of $\Delta m \geq 0$ and $m_{\Delta^{\pm\pm\pm}}$ for $v_\Delta = 10^{-6}$ GeV and $v_\Delta = 5 \times 10^{-3}$ GeV can be discovered with the integrated luminosities of 3.3 fb^{-1} and 110 fb^{-1}, respectively. Our studies promote the possibility of discovering new physics in searches for final states with at least three same-sign leptons without b-jet at the LHC and future 100 TeV pp colliders.

6 Conclusions

In this work, we have studied the potential of searching for triply charged Higgs bosons at the LHC and a 100 TeV pp collider. We first discuss the methodology of producing and detecting a multi-charged Higgs boson at pp colliders. While the singly and doubly charged Higgs bosons have been discussed thoroughly, the triply charged Higgs boson has not been paid much attention. The details of a specifically non-trivial model with a Higgs quadruplet and a pair of vector-like triplet leptons are given. The indirect constraints on this model are subsequently discussed, which indicate that the magnitude of mass splitting Δm between the nearby states of the Higgs quadruplet is restricted to be smaller than 30 GeV while the quadruplet VEV v_Δ larger (smaller) than 1.5×10^{-9} GeV (1.3 GeV) is allowed.

We then discuss the production cross section and decay branching ratio of the triply charged Higgs boson. With the increase of collider energy, the production cross section becomes larger significantly. This motivates us to study the sensitivity of searching for a triply charged Higgs bsons at a 100 TeV pp collider. Triply charged Higgs boson can

[9] The veto of b-tagged jets also depends on the b-tagging efficiency. Although the recommended b-tagging efficiency at the LHC by the CMS Collaboration [102] is lower than that at the FCC-hh, this does not have large impact since the most dominant background is WZ.

[10] From Fig. 12, imposing the cuts $|\eta_{e/\mu/b}| < 2.5$ and $|\eta_{e/\mu/b}| < 6$ does not make much difference for the signal we studied at the LHC.

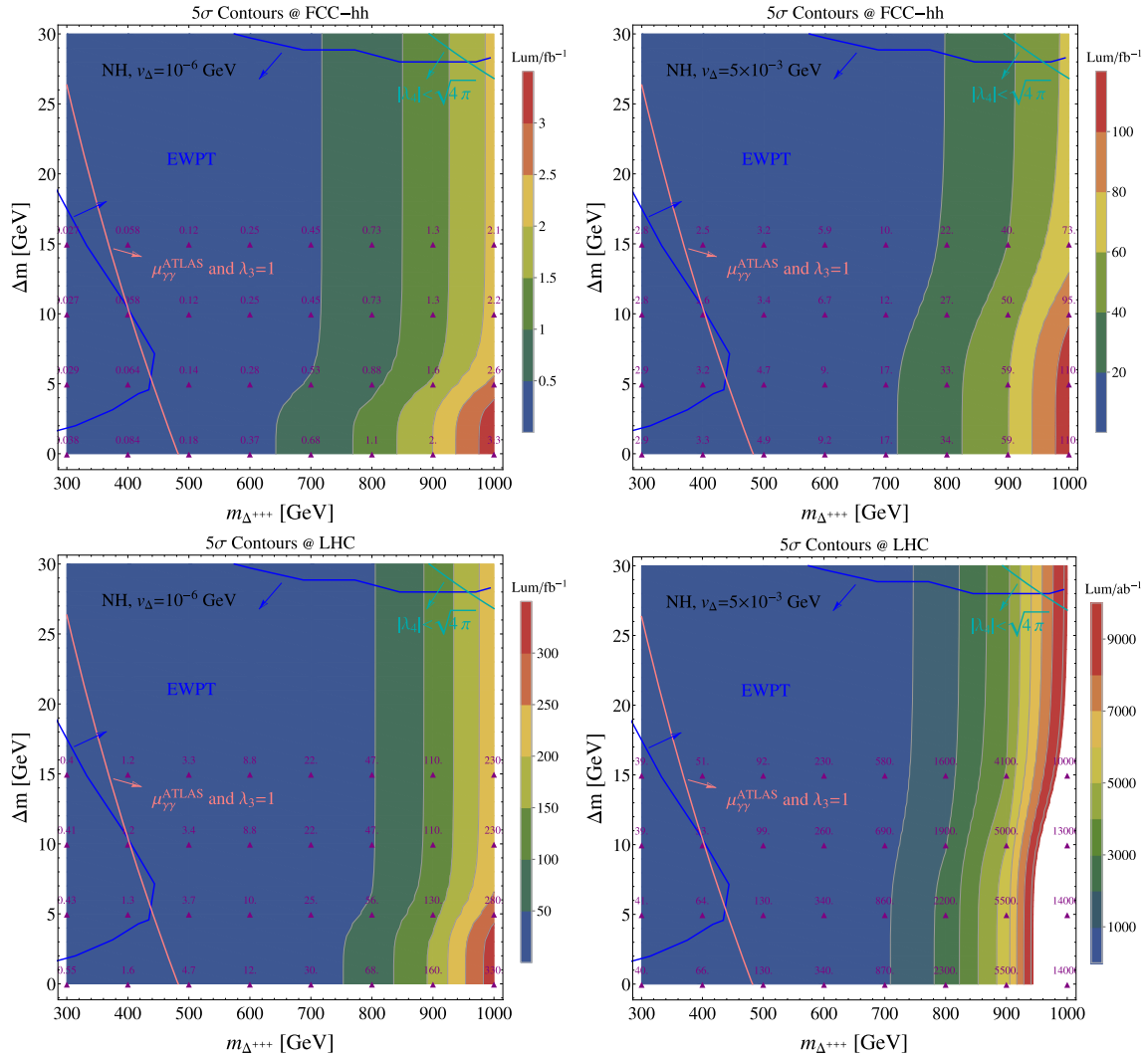

Fig. 13 5σ discovery prospects in the plane of $m_{\Delta^{\pm\pm\pm}}$ and Δm with the benchmark values of $v_\Delta = 10^{-6}$ GeV (left panels) and 5×10^{-3} GeV (right panels) for the NH at the 13 TeV LHC and FCC-hh. The contours correspond to the integrated luminosities (in units of fb^{-1}) required to satisfy $\mathcal{Z} = 5$. Benchmark points with $\Delta m = 1, 5, 10, 20$ GeV and $m_{\Delta^{\pm\pm\pm}} = 300$ GeV $-$ 1000 GeV are depicted in purple triangles with the numbers denoting the required integrated luminosities. The allowed regions from indirect constraints are also indicated

decay into $W^\pm W^\pm W^\pm$ or $\ell^\pm \ell^\pm W$ through an off-shell doubly charged Higgs boson with the decay branching ratios being nearly independent of the mass splitting Δm. The cascade decays are open if $\Delta m \neq 0$ and can be dominant in the medium region of v_Δ.

Thanks to the high charge, three same-sign leptons can be produced in the decays of triply charged Higgs boson. In previous studies with SS3L signature at the LHC, only part of SM backgrounds were considered. We consider a complete set of backgrounds, simulate them at a 100 TeV pp collider by taking the FCC-hh as an example and perform a detailed collider analysis with at least three same-sign leptons in the final state being selected, which is inclusive for the signal processes with one or two $\Delta^{\pm\pm\pm}$ and the decays $\Delta^{\pm\pm(\pm)} \to \ell^\pm \ell^{\pm\pm}(W^\pm)$ and $W^\pm W^\pm (W^\pm)$. The cascade decays giving rise to the SS3L signature for $\Delta m > 0$ are also properly included. Signal events are generated according to their dependence on the mass splitting Δm and the quadruplet VEV v_Δ, so that we can obtain the discovery significance as a function of v_Δ.

For a comparison, we choose two benchmark values of v_Δ, for which prompt searches are valid. We find that previous studies at the LHC underestimated the significance by several times. We revisit the sensitivity at the LHC by projecting that at the FCC-hh since the differential distributions at these two colliders are close except the rapidity distributions. Our study shows that 5σ discovery can be reached for a triply charged Higgs boson below 1 TeV with 330 fb^{-1} of data at the LHC for a relatively small $v_\Delta = 10^{-6}$ GeV and with 110 fb^{-1} of data at a 100 TeV pp collider in the whole region

1.5×10^{-9} GeV $\lesssim v_\Delta \lesssim$ 1.3 GeV for the mass splitting $\Delta m = 0$. For $\Delta m > 0$, the sensitivity is further improved due to the cascade decays.

Acknowledgements We thank Yong Du, Michael Ramsey-Musolf and Yi-Lei Tang for helpful discussions and comments. The valuable correspondence with Jung Chang, Tathagata Ghosh and Takaaki Nomura is also thankfully acknowledged. This work was supported in part by NSFC (Grants 11735010, 11975149, 12090064), by Key Laboratory for Particle Physics, Astrophysics and Cosmology, Ministry of Education, and Shanghai Key Laboratory for Particle Physics and Cosmology (Grant No. 15DZ2272100), and in part by the MOST (Grants No.109-2112-M-002-017-MY3.

Data Availability Statement This manuscript has no associated data or the data will not be deposited. [Authors' comment: All the data are already included in the main manuscript.]

Funded by SCOAP[3].

Appendix

Appendix A: The Z, $W^\pm$ masses and the would-be Goldstone modes

In this Appendix, we will give more details of the model with a SM Higgs doublet H and a Higgs multiplet H_n in Sect. 1 by expanding Eq. (1).

The VEV of H_n will modify the W and Z boson masses compared to the model with just H to have

$$m_W^2 = \frac{g^2}{4}(v_H^2 + 2(I_n(I_n+1) - Y_n^2)v_n^2) ,$$
$$m_Z^2 = \frac{g^2}{4c_W^2}(v_H^2 + 4Y_n^2 v_n^2) . \tag{A1}$$

where I_n is the isospin of the $SU(2)_L$ of a n-th rank Higgs representation. Therefore, the ρ parameter is expressed as

$$\rho = \frac{v_H^2 + 2(I_n(I_n+1) - Y_n^2)v_n^2}{v_H^2 + 4Y_n^2 v_n^2} . \tag{A2}$$

Experimentally, the ρ parameter is determined to be very close to unity, $\rho = 1.00039 \pm 0.00019$ [23]. In the usual Higgs representation, the VEV v_n is constrained to be small compared with the doublet VEV v_H. The new Higgs boson couplings to SM fermions are small proportional to v_n/v_H. If n is larger than 3, H_n does not couple to SM fermions directly for a Lagrangian that is renormalizable.

The Goldstone bosons and charged Higgs fields of H_n are

$$G_Z = \frac{v_H I^0 + 2Y_n v_n I_n^0}{\sqrt{v_H^2 + 4Y_n^2 v_n^2}} ,$$
$$G_W^+ = \frac{v_H h^+ + v_n\sqrt{2(I_n(I_n+1) - Y_n^2)}\phi^+}{\sqrt{v_H^2 + v_n^2 2(I_n(I_n+1) - Y_n^2)}} , \tag{A3}$$

where h^+ denotes the singly charged field from the doublet representation H.

After removing the Goldstone bosons, one can obtain the physical pseudoscalar A^0 and singly charged Higgs bosons h_i^+ as given by

$$A^0 = \frac{2Y_n v_n I^0 - v_H I_n^0}{\sqrt{v_H^2 + 4Y_n^2 v_n^2}} , \tag{A4}$$

and

$$h_1^+ = \frac{v_n\sqrt{2(I_n(I_n+1) - Y_n^2)}h^+ - v_H\varphi^+}{\sqrt{v_H^2 + v_n^2 2(I_n(I_n+1) - Y_n^2)}} ,$$
$$h_2^+ = \frac{\sqrt{(I_n + Y_n + 1)(I_n - Y_n)}h_n^+ + \sqrt{(I_n - Y_n + 1)(I_n + Y_n)}h_n^{-*}}{\sqrt{2(I_n(I_n+1) - Y_n^2)}} , \tag{A5}$$

with φ^+ given by

$$\varphi^+ = \frac{\sqrt{(I_n - Y_n + 1)(I_n + Y_n)}h_n^+ - \sqrt{(I_n + Y_n + 1)(I_n - Y_n)}h_n^{-*}}{\sqrt{2(I_n(I_n+1) - Y_n^2)}} , \tag{A6}$$

Note that h_i^+ may or may not be mass eigenstates depending on the details of Higgs potential. For simplicity, we will assume that they are mass eigenstates.

It is convenient to write the two real neutral components h^0 and h_n^0 as

$$h_1^0 = \frac{v_H h^0 + 2Y_n v_n h_n^0}{\sqrt{v_H^2 + 4Y_n^2 v_n^2}} , \quad h_2^0 = \frac{2Y_n v_n h^0 - v_H h_n^0}{\sqrt{v_H^2 + 4Y_n^2 v_n^2}} . \tag{A7}$$

In general, h^0, h^+, h_n^0 and $h_n^{Q=1}$ are not mass eigenstates. From Eqs. (A3), (A4), (A5) and (A7), the mass eigenstates can be written as the following basis transformations. For real neutral fields h_α ($h_1 \equiv h^0$, $h_2 \equiv h_n^0$)

$$h_\alpha = \sum_{\alpha,\beta=1}^{3} (N_R)_{\alpha\beta} h_\beta^{m0} , \tag{A8}$$

where N_R denotes the 2×2 orthogonal matrix and h_α^{m0} are the mass eigenstates ($h_{1(2)}^{m0} \equiv h_{1(2)}^0$). For imaginary neutral

Table 3 Feynman Rules. All momenta flow into the vertex

Vertices	Coefficients
$W_\mu^\pm h_\alpha^{m0} H_\beta^{m\mp}$	$i\frac{g_2}{2}((N_R)_{1\alpha}S_{1\beta} - \sqrt{(I_n - Y_n)(I_n + Y_n + 1)}(N_R)_{2\alpha}S_{2\beta}$
	$+\sqrt{(I_n + Y_n)(I_n - Y_n + 1)}(N_R)_{2\alpha}S_{3\beta})(P_2 - P_1)_\mu$
$W_\mu^\pm A^0 H_\beta^{m\mp}$	$-\frac{g_2}{2}((N_I)_{12}S_{1\beta} + \sqrt{(I_n - Y_n)(I_n + Y_n + 1)}(N_I)_{22}S_{2\beta}$
	$+\sqrt{(I_n + Y_n)(I_n - Y_n + 1)}(N_I)_{22}S_{3\beta})(P_2 - P_1)_\mu$
$W_\mu^+ H_\beta^{m+} h_n^{2*}$	$i\frac{g_2}{\sqrt{2}}\sqrt{(I_n - Y_n + 2)(I_n + Y_n - 1)}S_{3\beta}(P_2 - P_1)_\mu$
$W_\mu^+ H_\beta^{m+} h_n^{-2}$	$i\frac{g_2}{\sqrt{2}}\sqrt{(I_n - Y_n + 2)(I_n + Y_n - 1)}S_{2\beta}(P_2 - P_1)_\mu$
$W_\mu^+ h_n^Q h_n^{Q+1*}, (Q \geq 2)$	$i\frac{g_2}{\sqrt{2}}\sqrt{(I_n - Y_n + (Q+1))(I_n + Y_n - Q)}(P_2 - P_1)_\mu$
$W_\mu^+ h_n^{-Q*} h_n^{-(Q+1)}, (Q \geq 2)$	$i\frac{g_2}{\sqrt{2}}\sqrt{(I_n - Y_n - Q)(I_n + Y_n + (Q+1))}(P_2 - P_1)_\mu$
$Z_\mu Z^\mu h_\alpha^{m0}$	$\frac{g_2^2}{4c_W^2}((N_R)_{1\alpha}v_H + 4Y_n^2(N_R)_{2\alpha}v_n)g_{\mu\nu}$
$Z_\mu Z^\mu h_\alpha^{m0} h_\alpha^{m0}$	$\frac{g_2^2}{8c_W^2}((N_R)_{1\alpha}^2 + 4Y_n^2(N_R)_{2\alpha}^2)g_{\mu\nu}$
$Z_\mu Z^\mu A^0 A^0$	$\frac{g_2^2}{8c_W^2}((N_I)_{12}^2 + 4Y_n^2(N_I)_{22}^2)g_{\mu\nu}$
$A_\mu A^\mu H_\alpha^{m\pm} H_\alpha^{m\mp}$	$((S_{1\alpha})^2 + (S_{2\alpha})^2 + (S_{3\alpha})^2)e^2 g_{\mu\nu}$
$A_\mu Z^\mu H_\alpha^{m\pm} H_\alpha^{m\mp}$	$\frac{2eg_2}{c_W}((c_W^2 - \frac{1}{2})(S_{1\alpha})^2 + (c_W^2 + Y_n)(S_{2\alpha})^2 + (c_W^2 - Y_n)(S_{3\alpha})^2)g_{\mu\nu}$
$Z_\mu Z^\mu H_\alpha^{m\pm} H_\alpha^{m\mp}$	$\frac{g_2^2}{c_W^2}((c_W^2 - \frac{1}{2})^2(S_{1\alpha})^2 + (c_W^2 + Y_n)^2(S_{2\alpha})^2 + (c_W^2 - Y_n)^2(S_{3\alpha})^2)g_{\mu\nu}$
$A_\mu A^\mu h_n^{(-)Q*} h_n^{(-)Q}, (Q \geq 2)$	$Q^2 e^2 g_{\mu\nu}$
$A_\mu Z^\mu h_n^{(-)Q*} h_n^{(-)Q}, (Q \geq 2)$	$\frac{2Qeg_2}{c_W}(Qc_W^2 - (+)Y_n)g_{\mu\nu}$
$Z_\mu Z^\mu h_n^{(-)Q*} h_n^{(-)Q}, (Q \geq 2)$	$\frac{g_2^2}{c_W^2}(Qc_W^2 - (+)Y_n)^2 g_{\mu\nu}$
$Z_\mu h_\alpha^{m0} h_\beta^{m0}$	$-i\frac{g_2}{4c_W}((N_R)_{1\alpha}(N_R)_{1\beta} + 2Y_n(N_R)_{2\alpha}(N_R)_{2\beta})(P_2 - P_1)_\mu$
$Z_\mu A^0 A^0$	$-i\frac{g_2}{4c_W}((N_I)_{12}^2 + 2Y_n(N_I)_{22}^2)(P_2 - P_1)_\mu$
$A_\mu H_\alpha^{m\pm} H_\beta^{m\mp}$	$ie(S_{1\alpha}S_{1\beta} + S_{2\alpha}S_{2\beta} + S_{3\alpha}S_{3\beta})(P_2 - P_1)_\mu$
$Z_\mu H_\alpha^{m\pm} H_\beta^{m\mp}$	$i\frac{g_2}{2c_W}((2c_W^2 - 1)S_{1\alpha}S_{1\beta} + 2(c_W^2 + Y_n)S_{2\alpha}S_{2\beta}$
	$+2(c_W^2 - Y_n)S_{3\alpha}S_{3\beta})(P_2 - P_1)_\mu$
$A_\mu h_n^{(-)Q} h_n^{(-)Q*}, (Q \geq 2)$	$(-)iQe(P_2 - P_1)_\mu$
$Z_\mu h_n^{(-)Q} h_n^{(-)Q*}, (Q \geq 2)$	$(-)i\frac{g_2}{c_W}(Qc_W^2 - (+)Y_n)(P_2 - P_1)_\mu$

fields I_α ($I_1 \equiv I^0$, $I_2 \equiv I_n^0$)

$$I_\alpha = \sum_{\alpha,\beta=1}^{3} (N_I)_{\alpha\beta} I_\beta^m \ , \tag{A9}$$

where N_I denotes the 2×2 orthogonal matrix and I_α^m are the mass eigenstates. $I_1^m \equiv G_Z$ is the would-be Goldstone boson and $I_2^m \equiv A^0$. For singly charged fields H_α^+ ($H_1^+ \equiv h^+$, $H_2^+ \equiv h_n^{-*}$, $H_3^+ \equiv h_n^+$)[11]

$$H_\alpha^+ = \sum_{\alpha,\beta=1}^{3} S_{\alpha\beta} H_\beta^{m+} \ , \tag{A10}$$

where S denotes the 3×3 orthogonal matrix and H_β^{m+} denotes the mass eigenstates. $H_1^{m+} \equiv G_W^+$ is the would-be Goldstone boson and the physical Higgs bosons $H_{2(3)}^{m+} \equiv h_{1(2)}^+$.

[11] In general, $h_n^{|Q|-*} \neq h_n^{|Q|}$. The equality only holds for real representations.

Appendix B: Feynman rules in the general Higgs representation

The production and detection additional Higgs boson depend on their couplings to photon, $W^\pm$ and Z bosons. Using Eq. (1), we have the following interaction terms relevant to A, $W^\pm$ and Z fields ($g_2 \equiv g$ is the $SU(2)_L$ gauge coupling),

$$\mathcal{L}_{\rm int}^W = i\frac{g_2}{\sqrt{2}} \Big[\sqrt{(I_n + m)(I_n - m + 1)}\partial^\mu (h_n^Q)^* h_n^{Q-1} - \sqrt{(I_n - m)(I_n + m + 1)}\partial^\mu h_n^Q (h_n^{Q+1})^*\Big]$$

Table 4 Feynman Rules (continued)

Vertices	Coefficients
$W_\mu^- W^{\mu+} h_\alpha^{m0} h_\alpha^{m0}$	$\frac{g_2^2}{4}((N_R)_{1\alpha}^2 + (I_n(I_n+1) - Y_n^2)(N_R)_{2\alpha}^2) g_{\mu\nu}$
$W_\mu^- W^{\mu+} h_\alpha^{m0}$	$\frac{g_2^2}{2}((N_R)_{1\alpha} v_H + (I_n(I_n+1) - Y_n^2)(N_R)_{2\alpha} v_n) g_{\mu\nu}$
$W_\mu^- W^{\mu+} A^0 A^0$	$\frac{g_2^2}{4}((N_I)_{12}^2 + (I_n(I_n+1) - Y_n^2)(N_I)_{22}^2) g_{\mu\nu}$
$W_\mu^- W^{\mu+} H_\alpha^{m\pm} H_\alpha^{m\mp}$	$\frac{g_2^2}{2}(S_{1\alpha}^2 + (I_n(I_n+1) - (1+Y_n)^2) S_{2\alpha}^2 + (I_n(I_n+1) - (1-Y_n)^2) S_{3\alpha}^2) g_{\mu\nu}$
$W_\mu^- W^{\mu+} h_n^{Q,*} h_n^Q$,$(\|Q\| \geq 2)$	$\frac{g_2^2}{2}(I_n(I_n+1) - (Q - Y_n)^2) g_{\mu\nu}$
$W_\mu^- W^{\mu-} h_\alpha^{m0} h_n^{(-)2(*)}$	$\frac{g_2^2}{2\sqrt{2}} \sqrt{(I_n^2 - (1-(+)Y_n)^2)((I_n+1)^2 - (1-(+)Y_n)^2)} (N_R)_{2\alpha} g_{\mu\nu}$
$W_\mu^- W^{\mu-} A^0 h_n^{(-)2(*)}$	$-(+)i \frac{g_2^2}{2\sqrt{2}} \sqrt{(I_n^2 - (1-(+)Y_n)^2)((I_n+1)^2 - (1-(+)Y_n)^2)} (N_I)_{22} g_{\mu\nu}$
$W_\mu^- W^{\mu-} h_n^{(-)2(*)}$	$\frac{g_2^2 v_n}{2\sqrt{2}} \sqrt{(I_n^2 - (1-(+)Y_n)^2)((I_n+1)^2 - (1-(+)Y_n)^2)} g_{\mu\nu}$
$W_\mu^- W^{\mu-} H_\alpha^{m-} h_n^{(-)3(*)}$	$\frac{g_2^2}{2} \sqrt{(I_n^2 - (2-(+)Y_n)^2)((I_n+1)^2 - (2-(+)Y_n)^2)} S_{(2)3\alpha} g_{\mu\nu}$
$W_\mu^- W^{\mu-} h_n^{Q*} h_n^{Q+2}$,	$\frac{g_2^2}{2} \sqrt{(I_n^2 - ((Q+1) - Y_n)^2)((I_n+1)^2 - ((Q+1) - Y_n)^2)} g_{\mu\nu}$
($Q \geq 2$ for positive Q & $Q \leq -4$ for negative Q)	

Table 5 Feynman Rules (continued). It is noted that there is no coupling of physical singly charged Higgs boson to $\gamma W^\pm$. After removing the would-be Goldstone boson, the interaction of $A_\mu W^{\mu\pm} H_\beta^{m\mp}$ becomes vanishing

Vertices	Coefficients
$A_\mu W^{\mu\mp} h_\alpha^{m0} H_\beta^{m\pm}$	$\frac{eg_2}{2}((N_R)_{1\alpha} S_{1\beta} - \sqrt{(I_n + Y_n + 1)(I_n - Y_n)} (N_R)_{2\alpha} S_{2\beta}$ $+\sqrt{(I_n - Y_n + 1)(I_n + Y_n)} (N_R)_{2\alpha} S_{3\beta}) g_{\mu\nu}$
$A_\mu W^{\mu\mp} A^0 H_\beta^{m\pm}$	$-i \frac{eg_2}{2}((N_I)_{12} S_{1\beta} + \sqrt{(I_n + Y_n + 1)(I_n - Y_n)} (N_I)_{22} S_{2\beta}$ $+\sqrt{(I_n - Y_n + 1)(I_n + Y_n)} (N_I)_{22} S_{3\beta}) g_{\mu\nu}$
$Z_\mu W^{\mu\mp} H_\beta^{m\pm}$	$-\frac{g_2^2}{2c_W}(s_W^2 v_H S_{1\beta} + (c_W^2 + 2Y_n)\sqrt{(I_n - Y_n)(I_n + Y_n + 1)} v_n S_{2\beta}$ $-(c_W^2 - 2Y_n)\sqrt{(I_n + Y_n)(I_n - Y_n + 1)} v_n S_{3\beta}) g_{\mu\nu}$
$Z_\mu W^{\mu\mp} h_\alpha^{m0} H_\beta^{m\pm}$	$-\frac{g_2^2}{2c_W}(s_W^2 (N_R)_{1\alpha} S_{1\beta} + (c_W^2 + 2Y_n)\sqrt{(I_n - Y_n)(I_n + Y_n + 1)} (N_R)_{2\alpha} S_{2\beta}$ $-(c_W^2 - 2Y_n)\sqrt{(I_n + Y_n)(I_n - Y_n + 1)} (N_R)_{2\alpha} S_{3\beta}) g_{\mu\nu}$
$Z_\mu W^{\mu\mp} A^0 H_\beta^{m\pm}$	$i \frac{g_2^2}{2c_W}(s_W^2 (N_I)_{12} S_{1\beta} - (c_W^2 + 2Y_n)\sqrt{(I_n - Y_n)(I_n + Y_n + 1)} (N_I)_{22} S_{2\beta}$ $-(c_W^2 - 2Y_n)\sqrt{(I_n + Y_n)(I_n - Y_n + 1)} (N_I)_{22} S_{3\beta}) g_{\mu\nu}$
$A_\mu W^{\mu-} h_n^2 H_\alpha^{m-}$	$3\frac{eg_2}{\sqrt{2}} \sqrt{(I_n + Y_n - 1)(I_n - Y_n + 2)} S_{3\alpha} g_{\mu\nu}$
$A_\mu W^{\mu-} h_n^{-2*} H_\alpha^{m-}$	$-3\frac{eg_2}{\sqrt{2}} \sqrt{(I_n - Y_n - 1)(I_n + Y_n + 2)} S_{2\alpha} g_{\mu\nu}$
$Z_\mu W^{\mu-} h_n^2 H_\alpha^{m-}$	$\frac{g_2^2}{\sqrt{2}c_W}(3c_W^2 - 2Y_n)\sqrt{(I_n + Y_n - 1)(I_n - Y_n + 2)} S_{3\alpha} g_{\mu\nu}$
$Z_\mu W^{\mu-} h_n^{-2*} H_\alpha^{m-}$	$-\frac{g_2^2}{\sqrt{2}c_W}(3c_W^2 + 2Y_n)\sqrt{(I_n - Y_n - 1)(I_n + Y_n + 2)} S_{2\alpha} g_{\mu\nu}$
$A_\mu W^{\mu-} h_n^{Q*} h_n^{Q+1}$,	$\frac{eg_2}{\sqrt{2}}(2Q+1)\sqrt{(I_n + Y_n - Q)(I_n - Y_n + (Q+1))} g_{\mu\nu}$
($Q \geq 2$ for positive Q & $Q \leq -3$ for negative Q)	
$Z_\mu W^{\mu-} h_n^{Q*} h_n^{Q+1}$,	$\frac{g_2^2}{\sqrt{2}c_W}((2Q+1)c_W^2 - 2Y_n)\sqrt{(I_n + Y_n - Q)(I_n - Y_n + (Q+1))} g_{\mu\nu}$
($Q \geq 2$ for positive Q & $Q \leq -3$ for negative Q)	

$$
\begin{aligned}
& W_\mu^+ + \text{H.C.}\,, \\
\mathcal{L}_{\text{int}}^{A,Z} &= i\left(\partial^\mu (h_n^Q)^* h_n^Q - \partial^\mu h_n^Q (h_n^Q)^*\right) \\
& (eQA_\mu + \frac{g_2}{c_W}(m - Qs_W^2)Z_\mu)\,, \\
\mathcal{L}_{\text{int}}^{WW} &= \frac{g_2^2}{2} \\
& \Big[(I_n + m)(I_n - m + 1)(h_n^{Q-1})^* h_n^{Q-1} \\
& \quad + (I_n - m)(I_n + m + 1)(h_n^{Q+1})^* h_n^{Q+1}\Big] \\
& W^{+\mu} W_\mu^-\,, \\
& + \sqrt{(I_n^2 - m^2)((I_n + 1)^2 - m^2)} \\
& \Big[W^{-\mu} W_\mu^- (h_n^{Q-1})^* h_n^{Q+1} + \text{H.C.}\Big]\,, \\
\mathcal{L}_{\text{int}}^{AA,ZZ,AZ} &= (eQA_\mu + \frac{g_2}{c_W} \\
& (m - Qs_W^2)Z_\mu)^2 (h_n^Q)^* h_n^Q\,, \\
\mathcal{L}_{\text{int}}^{WA,WZ} &= \frac{g_2}{\sqrt{2}}(eQA^\mu + \frac{g_2}{c_W}(m - Qs_W^2)Z^\mu) \\
& \Big[W_\mu^- (\sqrt{(I_n + m)(I_n - m + 1)}(h^{Q-1})^* h_n^Q \\
& \quad + \sqrt{(I_n - m)(I_n + m + 1)}(h_n^Q)^* h_n^{Q+1} \\
& \quad + \text{H.C.})]\,. \qquad \text{(B1)}
\end{aligned}
$$

Substituting the physical components defined in Appendix A into Eq. (B1), one can get the Feynman rules of Higgs-Gauge couplings. We list the tables of Feynman rules in the following. Note that we have removed the would-be Goldstone bosons G_Z and $G_W^\pm$ after the electroweak symmetry breaking, thus $\alpha = 2, 3$ for the singly charged Higgs field $H_\alpha^{m\pm}$.

References

1. G. Aad et al. (ATLAS), Phys. Lett. B **716**, 1 (2012). arXiv:1207.7214
2. S. Chatrchyan et al. (CMS), Phys. Lett. B **716**, 30 (2012). arXiv:1207.7235
3. G.C. Branco, P.M. Ferreira, L. Lavoura, M.N. Rebelo, M. Sher, J.P. Silva, Phys. Rep. **516**, 1 (2012). arXiv:1106.0034
4. S.P. Martin, pp. 1–98 (1997), [Adv. Ser. Direct. High Energy Phys.18,1 (1998)], arXiv:hep-ph/9709356
5. M.P. Bento, H.E. Haber, J.C. Romão, J.P. Silva, JHEP **11**, 095 (2017). arXiv:1708.09408
6. M.P. Bento, H.E. Haber, J.C. Romão, J.P. Silva, JHEP **10**, 143 (2018). arXiv:1808.07123
7. R.N. Mohapatra, G. Senjanovic, Phys. Rev. D **23**, 165 (1981)
8. J. Schechter, J.W.F. Valle, Phys. Rev. D **22**, 2227 (1980)
9. T.P. Cheng, L.-F. Li, Phys. Rev. D **22**, 2860 (1980)
10. G. Lazarides, Q. Shafi, C. Wetterich, Nucl. Phys. B **181**, 287 (1981)
11. C. Wetterich, Nucl. Phys. B **187**, 343 (1981)
12. P. Fileviez Perez, T. Han, G.-Y. Huang, T. Li, K. Wang, Phys. Rev. D **78**, 015018 (2008). arXiv:0805.3536
13. M. Aoki, S. Kanemura, K. Yagyu, Phys. Rev. D **85**, 055007 (2012). arXiv:1110.4625
14. K. Yagyu, Ph.D. thesis, Toyama U. (2012). arXiv:1204.0424
15. Z. Kang, J. Li, T. Li, Y. Liu, G.-Z. Ning, Eur. Phys. J. C **75**, 574 (2015). arXiv:1404.5207
16. M. Cirelli, N. Fornengo, A. Strumia, Nucl. Phys. B **753**, 178 (2006). arXiv:hep-ph/0512090
17. W. Chao, G.-J. Ding, X.-G. He, M. Ramsey-Musolf, JHEP **08**, 058 (2019). arXiv:1812.07829
18. T. Han, B. Mukhopadhyaya, Z. Si, K. Wang, Phys. Rev. D **76**, 075013 (2007). arXiv:0706.0441
19. M. Drees, R.M. Godbole, M. Nowakowski, S.D. Rindani, Phys. Rev. D **50**, 2335 (1994). arXiv:hep-ph/9403368
20. K.S. Babu, S. Jana, Phys. Rev. D **95**, 055020 (2017). arXiv:1612.09224
21. J.A. Grifols, A. Mendez, Phys. Rev. D **22**, 1725 (1980)
22. J.F. Gunion, H.E. Haber, G.L. Kane, S. Dawson, Front. Phys. **80**, 1 (2000)
23. M. Tanabashi et al., Particle Data Group. Phys. Rev. D **98**, 030001 (2018)
24. J. Hisano, K. Tsumura, Phys. Rev. D **87**, 053004 (2013). arXiv:1301.6455
25. M.-J. Harris, H.E. Logan, Phys. Rev. D **95**, 095003 (2017). arXiv:1703.03832
26. C.-W. Chiang, K. Yagyu, Phys. Lett. B **786**, 268 (2018). arXiv:1808.10152
27. A.G. Akeroyd et al., Eur. Phys. J. C **77**, 276 (2017). arXiv:1607.01320
28. Q.-H. Cao, G. Li, K.-P. Xie, J. Zhang, Phys. Rev. D **97**, 115036 (2018). arXiv:1711.02113
29. Q.-H. Cao, G. Li, K.-P. Xie, J. Zhang, Phys. Rev. D **99**, 015027 (2019). arXiv:1810.07659
30. J.-Y. Cen, J.-H. Chen, X.-G. He, G. Li, J.-Y. Su, W. Wang, JHEP **01**, 148 (2019). arXiv:1811.00910
31. Y. Du, A. Dunbrack, M.J. Ramsey-Musolf, J.-H. Yu, JHEP **01**, 101 (2019). arXiv:1810.09450
32. H. Georgi, M. Machacek, Nucl. Phys. B **262**, 463 (1985)
33. M.S. Chanowitz, M. Golden, Phys. Lett. **165B**, 105 (1985)
34. C.-W. Chiang, T. Nomura, K. Tsumura, Phys. Rev. D **85**, 095023 (2012). arXiv:1202.2014
35. C.-W. Chiang, A.-L. Kuo, T. Yamada, JHEP **01**, 120 (2016). arXiv:1511.00865
36. K.S. Babu, S. Nandi, Z. Tavartkiladze, Phys. Rev. D **80**, 071702 (2009). arXiv:0905.2710
37. G. Bambhaniya, J. Chakrabortty, S. Goswami, P. Konar, Phys. Rev. D **88**, 075006 (2013). arXiv:1305.2795
38. K. Ghosh, S. Jana, S. Nandi, JHEP **03**, 180 (2018a). arXiv:1705.01121
39. T. Ghosh, S. Jana, S. Nandi, Phys. Rev. D **97**, 115037 (2018b). arXiv:1802.09251
40. M. Aaboud et al. (ATLAS), JHEP **09**, 084 (2017). arXiv:1706.03731
41. T. A. collaboration (ATLAS), Tech. Rep. ATLAS-CONF-2019-005 (2019)
42. C. Collaboration (CMS), Tech. Rep. CMS-PAS-HIG-17-031 (2018)
43. A. Djouadi, Phys. Rept. **459**, 1 (2008). arXiv:hep-ph/0503173
44. M. Baak, M. Goebel, J. Haller, A. Hoecker, D. Kennedy, R. Kogler, K. Moenig, M. Schott, J. Stelzer, Eur. Phys. J. C **72**, 2205 (2012). arXiv:1209.2716
45. M.E. Peskin, T. Takeuchi, Phys. Rev. Lett. **65**, 964 (1990)
46. M.E. Peskin, T. Takeuchi, Phys. Rev. D **46**, 381 (1992)
47. T. Nomura, H. Okada (2019). arXiv:1903.05958
48. A.M. Baldini et al. (MEG), Eur. Phys. J. C **76**, 434 (2016). arXiv:1605.05081
49. W.H. Bertl et al. (SINDRUM II), Eur. Phys. J. C **47**, 337 (2006)

50. A.G. Akeroyd, M. Aoki, H. Sugiyama, Phys. Rev. D **79**, 113010 (2009). arXiv:0904.3640
51. D.N. Dinh, A. Ibarra, E. Molinaro, S.T. Petcov, JHEP **08**, 125 (2012). [Erratum: JHEP09,023(2013)], arXiv:1205.4671
52. M. Kakizaki, Y. Ogura, F. Shima, Phys. Lett. B **566**, 210 (2003). arXiv:hep-ph/0304254
53. R. Kitano, M. Koike, Y. Okada, Phys. Rev. D **66**, 096002 (2002). [Erratum: Phys. Rev. **D76**, 059902 (2007)]. arXiv:hep-ph/0203110
54. M. Aaboud et al. (ATLAS), Eur. Phys. J. **C78**, 199 (2018a). arXiv:1710.09748
55. C. Collaboration (CMS), Tech. Rep. CMS-PAS-HIG-16-036 (2017)
56. M. Aaboud et al. (ATLAS), Eur. Phys. J. **C79**, 58 (2019a). arXiv:1808.01899
57. V.M. Budnev, I.F. Ginzburg, G.V. Meledin, V.G. Serbo, Phys. Rep. **15**, 181 (1975)
58. F. Zimmermann, M. Benedikt, M. Capeans Garrido, F. Cerutti, B. Goddard, J. Gutleber, J. M. Jimenez, M. Mangano, V. Mertens, J. A. Osborne, et al., Tech. Rep. CERN-ACC-2018-0059, CERN, Geneva (2018), submitted for publication to Eur. Phys. J. ST., https://cds.cern.ch/record/2651305
59. X. Cid Vidal et al. (Working Group 3) (2018). arXiv:1812.07831
60. A. Abada et al. (FCC), Tech. Rep. CERN-ACC-2018-0058 (2019a)
61. A. Abada et al. (FCC), Eur. Phys. J. C **79**, 474 (2019b)
62. (2018). arXiv:1809.00285
63. M. Dong et al. (CEPC Study Group) (2018). arXiv:1811.10545
64. J. Alwall, R. Frederix, S. Frixione, V. Hirschi, F. Maltoni, O. Mattelaer, H.S. Shao, T. Stelzer, P. Torrielli, M. Zaro, JHEP **07**, 079 (2014). arXiv:1405.0301
65. R.D. Ball, V. Bertone, S. Carrazza, L. Del Debbio, S. Forte, A. Guffanti, N.P. Hartland, J. Rojo (NNPDF), Nucl. Phys. **B877**, 290 (2013). arXiv:1308.0598
66. M. Muhlleitner, M. Spira, Phys. Rev. D **68**, 117701 (2003). arXiv:hep-ph/0305288
67. Tech. Rep. ATLAS-CONF-2016-051, CERN, Geneva (2016). http://cds.cern.ch/record/2206133
68. Y. Cai, T. Han, T. Li, R. Ruiz, Front.in Phys. **6**, 40 (2018). arXiv:1711.02180
69. V. Bertone, S. Carrazza, N. P. Hartland, J. Rojo (NNPDF), SciPost Phys. **5**, 008 (2018). arXiv:1712.07053
70. I. Esteban, M.C. Gonzalez-Garcia, A. Hernandez-Cabezudo, M. Maltoni, T. Schwetz, JHEP **01**, 106 (2019). arXiv:1811.05487
71. T. A. collaboration (ATLAS), Tech. Rep. ATLAS-CONF-2016-042 (2016)
72. B. Mukhopadhyaya, S. Mukhopadhyay, Phys. Rev. D **82**, 031501 (2010). arXiv:1005.3051
73. S.K. Agarwalla, K. Ghosh, N. Kumar, A. Patra, JHEP **01**, 080 (2019). arXiv:1808.02904
74. C. Collaboration (CMS), Tech. Rep. CMS-PAS-TOP-18-003 (2019a)
75. C. Collaboration (CMS), Tech. Rep. CMS-PAS-SUS-19-008 (2019b)
76. V. Barger, W.-Y. Keung, B. Yencho, Phys. Lett. B **687**, 70 (2010). arXiv:1001.0221
77. M. Aaboud et al. (ATLAS), Phys. Rev. **D99**, 072009 (2019b). arXiv:1901.03584
78. V. Khachatryan et al. (CMS), Eur. Phys. J. **C76**, 439 (2016). arXiv:1605.03171
79. A. M. Sirunyan et al. (CMS), Eur. Phys. J. **C77**, 578 (2017). arXiv:1704.07323
80. D. Alva, T. Han, R. Ruiz, JHEP **02**, 072 (2015). arXiv:1411.7305
81. S. Mukhopadhyay, B. Mukhopadhyaya, Phys. Rev. D **84**, 095001 (2011). arXiv:1108.4921
82. T. Sjöstrand, S. Ask, J.R. Christiansen, R. Corke, N. Desai, P. Ilten, S. Mrenna, S. Prestel, C.O. Rasmussen, P.Z. Skands, Comput. Phys. Commun. **191**, 159 (2015). arXiv:1410.3012
83. T. Binoth, T. Gleisberg, S. Karg, N. Kauer, G. Sanguinetti, Phys. Lett. B **683**, 154 (2010). arXiv:0911.3181
84. F. Cascioli, T. Gehrmann, M. Grazzini, S. Kallweit, P. Maierhöfer, A. von Manteuffel, S. Pozzorini, D. Rathlev, L. Tancredi, E. Weihs, Phys. Lett. B **735**, 311 (2014). arXiv:1405.2219
85. M. Grazzini, S. Kallweit, D. Rathlev, M. Wiesemann, Phys. Lett. B **761**, 179 (2016). arXiv:1604.08576
86. T. Binoth, G. Ossola, C.G. Papadopoulos, R. Pittau, JHEP **06**, 082 (2008). arXiv:0804.0350
87. D.T. Nhung, L.D. Ninh, M.M. Weber, JHEP **12**, 096 (2013). arXiv:1307.7403
88. F. Campanario, V. Hankele, C. Oleari, S. Prestel, D. Zeppenfeld, Phys. Rev. D **78**, 094012 (2008). arXiv:0809.0790
89. V. Ahrens, A. Ferroglia, M. Neubert, B.D. Pecjak, L.L. Yang, Phys. Lett. B **703**, 135 (2011). arXiv:1105.5824
90. J.M. Campbell, R.K. Ellis, JHEP **07**, 052 (2012). arXiv:1204.5678
91. M.V. Garzelli, A. Kardos, C.G. Papadopoulos, Z. Trocsanyi, JHEP **11**, 056 (2012). arXiv:1208.2665
92. A. Lazopoulos, T. McElmurry, K. Melnikov, F. Petriello, Phys. Lett. B **666**, 62 (2008). arXiv:0804.2220
93. G. Bevilacqua, M. Worek, JHEP **07**, 111 (2012). arXiv:1206.3064
94. A. Bredenstein, A. Denner, S. Dittmaier, S. Pozzorini, Phys. Rev. Lett. **103**, 012002 (2009). arXiv:0905.0110
95. J. de Favereau, C. Delaere, P. Demin, A. Giammanco, V. Lemaître, A. Mertens, M. Selvaggi (DELPHES 3), JHEP **02**, 057 (2014). arXiv:1307.6346
96. C. Helsens, D. Jamin, M. L. Mangano, T. G. Rizzo, M. Selvaggi (2019). arXiv:1902.11217
97. F. Kling, H. Li, A. Pyarelal, H. Song, S. Su (2018). arXiv:1812.01633
98. M. Cacciari, G.P. Salam, G. Soyez, JHEP **04**, 063 (2008). arXiv:0802.1189
99. M. Cacciari, G.P. Salam, G. Soyez, Eur. Phys. J. C **72**, 1896 (2012). arXiv:1111.6097
100. M. Aaboud et al. (ATLAS), Eur. Phys. J. **C78**, 18 (2018b). arXiv:1710.11412
101. G. Cowan, K. Cranmer, E. Gross, O. Vitells, Eur. Phys. J. **C71**, 1554 (2011). [Erratum: Eur. Phys. J. **C73**, 2501 (2013)]. arXiv:1007.1727
102. S. Chatrchyan et al. (CMS), JINST **8**, P04013 (2013). arXiv:1211.4462